Activity-dependent inhibitory synapse scaling is determined by gephyrin phosphorylation and subsequent regulation of GABAA receptor diffusion

Sereina Battaglia, Marianne Renner, Marion Russeau, Etienne Côme, K. Tyagarajan Shiva, Sabine Lévi

1. Title: Activity-dependent inhibitory synapse scaling is determined by gephyrin phosphorylation and subsequent regulation of $GABA_A$ receptor diffusion.

2. Abbreviated Title: Gephyrin phosphorylation shapes $GABA_AR$ diffusion

3. Authors and affiliations :
Sereina Battaglia[4], Marianne Renner[1,2,3], Marion Russeau[1,2,3], Etienne Côme[1,2,3], Shiva K. Tyagarajan[4,5¥], Sabine Lévi[1,2,3¥]

[1] INSERM UMR-S 839, 75005, Paris, France
[2] Université Pierre et Marie Curie, 75005, Paris, France
[3] Institut du Fer a Moulin, 75005, Paris, France;
[4] Institute of Pharmacology and Toxicology, University of Zürich, 8057 Zurich, CH
[5] Center for Neuroscience Zurich, Winterthurerstrasse 190, 8057 Zurich, CH

[¥] co-senior authors

4. Author contributions:
SL and SKT conceptualized the project and designed the experiments. SL supervised the experimental work. SB, EC and M. Ru performed immunofluorescence and SPT experiments and analyzed the data together with SL. M. Ru prepared primary hippocampal neurons. MRe performed the super-resolution experiments, developed data analysis tools and analyzed the data. SL and SKT wrote the manuscript.

5. Correspondence should be addressed to:
Sabine Lévi
INSERM-UPMC UMR-S 839
17 rue du Fer a Moulin
75005 Paris, France
Tel. +33 1 45 87 61 13
E-mail: sabine.levi@inserm.fr

Shiva Tyagarajan
Institute of Pharmacology and Toxicology
University of Zürich
Winterthurerstrasse 190, 8057 Zurich, CH
Tel: +41 44 6355997
E-mail: tyagarajan@pharma.uzh.ch

6. Number of Figures : 8
7. Number of Tables : 0
8. Number of Multimedia : 0
9. Number of words for Abstract: 128
10. Number of words for Significance Statement: 36
11. Number of words for Introduction: 461
12. Number of words for Discussion: 1204

13. Acknowledgements:
We are grateful to the Cell and Tissue Imaging Facility of Institut du Fer à Moulin (IFM). This work was supported in part by INSERM, Sorbonne Université-UPMC, LabEx Biopsy to SL, Olgamyenfisch Grant to SKT and University of Zurich internal funding to SKT. EC is the recipient of a doctoral fellowship from the Université Pierre and Marie Curie. STORM/PALM equipment at the IFM was supported by DIM NeRF from Région Ile-de-France and by the FRC/Rotary 'Espoir en tête'. The Lévi lab is affiliated with the Paris School of Neuroscience (ENP) and the Bio-Psy Laboratory of excellence.

14. Conflict of interest:
No. The authors report no conflict of interest in relation to the submitted work.

15. Funding sources:
This work was supported in part by INSERM, Sorbonne Université-UPMC, LabEx Biopsy to SL, Olgamyenfisch Grant to SKT and University of Zurich internal funding to SKT. EC is the recipient of a doctoral fellowship from the Université Pierre and Marie Curie. STORM/PALM equipment at the IFM was supported by DIM NeRF from Région Ile-de-France and by the FRC/Rotary 'Espoir en tête'. The Lévi lab is affiliated with the Paris School of Neuroscience (ENP) and the Bio-Psy Laboratory of excellence.

Activity-dependent inhibitory synapse scaling is determined by gephyrin phosphorylation and subsequent regulation of $GABA_A$ receptor diffusion.

Abstract:

Synaptic plasticity relies on the rapid changes in neurotransmitter receptor number at postsynaptic sites. Using super resolution PALM imaging and quantum-dot based single particle tracking in rat hippocampal cultured neurons, we investigated if the phosphorylation status of the main scaffolding protein gephyrin influenced the organization of the gephyrin scaffold and $GABA_A$ receptor ($GABA_AR$) membrane dynamics. We found that gephyrin phosphorylation regulates gephyrin microdomain compaction. The ERK1/2 and GSK3β signaling alter the gephyrin scaffold mesh differentially. Differences in scaffold organization impacted similarly the diffusion of synaptic $GABA_ARs$, suggesting reduced gephyrin-receptor binding properties. In the context of synaptic scaling, our results identify a novel role of the GSK3β signaling pathway in the activity-dependent regulation of extrasynaptic receptor surface trafficking and GSK3β, PKA and CaMKIIα pathways in facilitating adaptations of synaptic receptors.

Significance Statement:

Our data identify phosphorylation as a key mechanism controlling the gephyrin scaffold mesh, and hence, the diffusion capture of $GABA_A$ receptors at inhibitory synapses. We further show how critical this mechanism is for inhibitory synaptic scaling.

Introduction:

Fast synaptic inhibition mediated by $GABA_A$Rs plays an essential role in information transfer between neurons. In recent years GABAergic inhibition has been shown to be dynamic, allowing flexible adaptations (Chen et al., 2012). Within the paradigm of in-vitro synaptic scaling, wherein the neuronal activity is pharmacologically manipulated for several hours to days, the effects of chronic changes in activity are still poorly understood at inhibitory synapses.

Neuronal inhibition is dynamically regulated by the amount of network activity. $GABA_A$R stability at synaptic sites and subsequent proteasomal degradation is an essential component of synaptic homeostasis that strongly influences amplitude and frequency of miniature inhibitory postsynaptic currents (mIPSCs) (Saliba et al., 2007). Similarly, lasting depolarization decreases $GABA_A$R internalization on principal neurons and increases GAD65 cluster size at presynaptic GABAergic terminals (Rannals and Kapur, 2011). These observations highlight that multiple systems and pathways facilitate inhibitory synapse adjustments in response to chronic changes in activity.

At postsynaptic sites lateral diffusion in and out of synapses can also rapidly alter receptor availability upon acute activity elevation (Bannai et al., 2009; 2015). Chemical induced long-term potentiation (iLTP) enhances phosphorylation of the $GABA_A$R β3 subunit at S383 by CaMKIIα, resulting in reduced surface mobility of $GABA_A$Rs, synaptic enrichment of receptors and increased inhibitory neurotransmission (Petrini et al., 2014). Hence, apart from endocytosis and exocytosis, lateral diffusion of receptors could also be an effective mechanism of synaptic plasticity.

In recent years it has become evident that the main scaffolding protein at the GABAergic synapse, gephyrin, is dynamically regulated, and this contributes to input-

specific adaptations at postsynaptic sites (Chen et al., 2012; van Versendaal et al., 2012; Villa et al., 2016). Identification of signaling pathways that converge onto gephyrin scaffolds by causing post-translational modifications of specific residues has shed new light into the molecular mechanisms underlying GABAergic synaptic plasticity. It was revealed that gephyrin phosphorylation by ERK1/2 at serine 268 (S268) reduces scaffold size and GABAergic mIPSC amplitude (Tyagarajan et al., 2013). Similarly, blocking GSK3β phosphorylation of gephyrin at serine 270 via the transgenic expression of the phospho-null mutant (S270A) significantly increases mIPSC frequency and amplitude (Tyagarajan et al., 2011). Theta burst stimulation (TBS) of CA3 Schaffer collaterals has been reported to induce gephyrin-mediated remodeling of GABAergic synapses in CA1 pyramidal cells (Flores et al., 2015). Although gephyrin phosphorylation at CaMKIIα sites is involved in this form of structural plasticity (Flores et al., 2015), the molecular basis for gephyrin phosphorylation induced $GABA_AR$ synapse dynamics remains to be further explored.

To address this we rendered gephyrin insensitive to ERK1/2 and GSK3β signaling pathways and studied their influence on $GABA_AR$ membrane diffusion properties. We report structural organization differences within gephyrin scaffolds based on their phosphorylation status. Furthermore, cooperation between gephyrin and $GABA_ARs$ are differentially regulated by gephyrin phosphorylation status and changes in activity.

Material and Methods

Neuronal culture

Primary cultures of hippocampal neurons were prepared from hippocampi dissected at embryonic day 18 or 19 from Sprague-Dawley rats of either sex. Tissue was then trypsinized (0.25% v/v), and mechanically dissociated in 1x HBSS (Invitrogen, Cergy Pontoise, France) containing 10 mM HEPES (Invitrogen). Neurons were plated at a density of 120 × 10^3 cells/ml onto 18-mm diameter glass coverslips (Assistent, Winigor, Germany) pre-coated with 50 µg/ml poly-D,L-ornithine (Sigma-Aldrich, Lyon, France) in plating medium composed of Minimum Essential Medium (MEM, Sigma) supplemented with horse serum (10% v/v, Invitrogen), L-glutamine (2 mM) and Na+ pyruvate (1 mM) (Invitrogen). After attachment for 3-4 h, cells were incubated in culture medium that consists of Neurobasal medium supplemented with B27 (1X), L-glutamine (2 mM), and antibiotics (penicillin 200 units/ml, streptomycin, 200 µg/ml) (Invitrogen) for up to 4 weeks at 37°C in a 5% CO2 humidified incubator. Each week, one fifth of the culture medium volume was replaced.

DNA constructs

The following constructs were used: *GEPHN* 3'-UTR shRNA and control shRNA-3m (Yu et al., 2007), DsRed-homer1c (Bats et al., 2007) (kindly provided by D. Choquet, IIN, Bordeaux, France), eGFP-gephyrin P1 variant (Lardi-Studler et al., 2007), and eGFP- or pDendra2- WT, -S268E, S270A, -DN, -S303A/S305A (SSA) and –SSA/S270A point mutants were generated using the eGFP-gephryin P1 variant as template for site directed mutagenesis (Tyagarajan et al., 2011; 2013; Flores et al., 2015).

Neuronal transfection

Transfections were carried out at DIV 14-15 using Lipofectamine 2000 (Invitrogen) or Transfectin (BioRad, Hercules, USA), according to the manufacturers' instructions (DNA:transfectin ratio 1 µg:3 µl), with 1-1.2 µg of plasmid DNA per 20 mm well. The following ratios of plasmid DNA were used in co-transfection experiments: 0.5:0.5:0.3 µg for eGFP-S268E/eGFP-S270A/eGFP-DN/eGFP-SSA/eGFP-SSA/S270A: *GEPHN* 3' UTR shRNA/*GEPHN* 3' UTR-3m shRNA: DsRed-homer1c. Experiments were performed 6 to 9 days post-transfection.

Pharmacology

4-aminopyridine (4-AP, 100 mM, Sigma) was directly added to the culture medium and the neurons were returned to a 5% CO2 humidified incubator for 8 or 48 h before use. For SPT experiments, neurons were labeled at 37°C in imaging medium (see below for composition) in presence of 4-AP, transferred to a recording chamber and recorded within 45 min at 31°C in imaging medium in the presence of 4-AP. The imaging medium consisted of phenol red-free minimal essential medium supplemented with glucose (33 mM; Sigma) and HEPES (20 mM), glutamine (2 mM), Na^+-pyruvate (1 mM), and B27 (1X) from Invitrogen.

Immunocytochemistry

Cells were fixed for 15 min at room temperature (RT) in paraformaldehyde (PFA, 4% w/v, Sigma) and sucrose (14% w/v, Sigma) solution prepared in PBS (1X). Following washes in PBS, cells were permeabilized with Triton (0.25% v/v, Sigma) diluted in PBS. Cells were washed again in PBS and incubated for 1 h at RT in Triton (0.1% v/v, Sigma) and goat serum (GS, 10% v/v, Invitrogen) in PBS to block nonspecific staining.

Subsequently, neurons were incubated for 1 h with a primary antibody mix consisting of guinea pig antibodies against $GABA_AR$ α2 subunit (1:2000, provided by J.M. Fritschy, Univ. Zurich) and rabbit anti-VGAT (1:400, provided by B. Gasnier, Univ. Paris Descartes, Paris) in PBS supplemented with GS (10% v/v, Invitrogen) and Triton (0.1%v/v, Sigma). After washes, cells were incubated for 60 min at RT with a secondary antibody mix containing biotinylated F(ab′)2 anti-guinea pig (1:300, Jackson Immunoresearch) and AMCA350-conjugated goat anti rabbit (1:100, Jackson Laboratories) in PBS-GS-Triton blocking solution, washed, incubated for another 45 min with streptavidin-CY5 (1:300, ThermoFisher) and finally mounted on glass slides using Mowiol 4-88 (48 mg/ml, Sigma). Sets of neurons compared for quantification were labeled simultaneously.

Fluorescence image acquisition and analysis

Image acquisition was performed using a 63 X objective (NA 1.32) on a Leica (Nussloch, Germany) DM6000 upright epifluorescence microscope with a 12-bit cooled CCD camera (Micromax, Roper Scientific) run by MetaMorph software (Roper Scientific, Evry, France). Quantification was performed using MetaMorph software (Roper Scientific). Image exposure time was determined on bright cells to obtain best fluorescence to noise ratio and to avoid pixel saturation. All images from a given culture were then acquired with the same exposure time and acquisition parameters. For each image, several dendritic regions of interest were manually chosen and a user-defined intensity threshold was applied to select clusters and avoid their coalescence. For quantification of gephyrin or $GABA_AR$ α2 synaptic clusters, gephyrin or receptor clusters comprising at least 3 pixels and colocalized on at least 1 pixel with VGAT

clusters were considered. The integrated fluorescence intensities of clusters were measured.

Live cell staining for single particle imaging

Neurons were incubated for 3-5 min at 37°C with primary antibodies against extracellular epitopes of $GABA_AR$ α2 subunit (guinea pig, 1:750/1:1000 provided by J.M. Fritschy), washed, and incubated for 3-5 min at 37°C with biotinylated Fab secondary antibodies (goat anti-guinea pig, 4-12µg/ml; Jackson Immuno research, West Grove, USA) in imaging medium. After washes, cells were incubated for 1 min with streptavidin-coated quantum dots (QDs) emitting at 605 nm (1 nM; Invitrogen) in borate buffer (50 mM) supplemented with sucrose (200 mM) or in PBS (1M; Invitrogen) supplemented with 10% Casein (v/v) (Sigma). Washing and incubation steps were all done in imaging medium. To assess the membrane dynamics of $GABA_AR$ α2 subunit at inhibitory synapses in neurons expressing the eGFP-DN mutant, inhibitory synapses were stained by incubating live neurons for 48 h at 37°C in a 5% CO2 humidified incubator with a primary VGAT antibody directly coupled to Oyster550 (1:200, Synaptic Systems) diluted in conditioned maintenance medium.

Single particle tracking and analysis

Cells were imaged using an Olympus IX71 inverted microscope equipped with a 60X objective (NA 1.42; Olympus) and a Lambda DG-4 monochromator (Sutter Instrument). Individual images of gephyrin-eGFP and homer1c-GFP, and QD real time recordings (integration time of 75 ms over 600 consecutive frames) were acquired with Hamamatsu ImagEM EMCCD camera and MetaView software (Meta Imaging 7.7). Cells were imaged within 45 min following labeling.

QD tracking and trajectory reconstruction were performed with Matlab software (The Mathworks, Natick, MA). One to two sub-regions of dendrites were quantified per cell. In cases of QD crossing, the trajectories were discarded from analysis. Trajectories were considered synaptic when overlapping with the synaptic mask of gephyrin-eGFP or VGAT-Oyster550 clusters, or extrasynaptic for spots two pixels (380 nm) away (Lévi et al., 2008). Values of the mean square displacement (MSD) plot versus time were calculated for each trajectory by applying the relation:

$$MSD(n\tau) = \frac{1}{N-n}\sum_{i=1}^{N-n}\left[\left(x((i+n)\tau) - x(i\tau)\right)^2 + \left(y((i+n)\tau) - y(i\tau)\right)^2\right]$$

(Saxton and Jacobson, 1997), where τ is the acquisition time, N is the total number of frames, n and i are positive integers with n determining the time increment. Diffusion coefficients (D) were calculated by fitting the first four points without origin of the MSD versus time curves with the equation: $MSD(n\tau) = 4Dn\tau + b$ where b is a constant reflecting the spot localization accuracy. Synaptic dwell time was defined as the duration of detection of QDs at synapses on a recording divided by the number of exits as detailed previously (Ehrensperger et al., 2007; Charrier et al., 2010). Dwell times ≤5 frames were not retained. The explored area of each trajectory was defined as the MSD value of the trajectory at two different time intervals of at 0.42 and 0.45 s (Renner et al., 2012).

PALM imaging

PALM imaging on fixed samples was carried out on an inverted N-STORM Nikon Eclipse Ti microscope with a 100x oil-immersion objective (N.A. 1.49) and an Andor iXon Ultra EMCCD camera (image pixel size, 160 nm), using specific lasers for PALM imaging of Dendra2 (405 and 561 nm). Movies of 10000 frames were acquired at frame

rates of 50 ms. The z position was maintained during acquisition by a Nikon perfect focus system. Single-molecule localization and 2D image reconstruction was conducted as described in (Specht et al., 2013) by fitting the PSF of spatially separated fluorophores to a 2D Gaussian distribution. The position of fluorophore were corrected by the relative movement of the synaptic cluster by calculating the center of mass of the cluster throughout the acquisition using a partial reconstruction of 2000 frames with a sliding window (Specht et al., 2013). PALM images were rendered by superimposing the coordinates of single-molecule detections, which were represented with 2D Gaussian curves of unitary intensity and SDs representing the localization accuracy (sigma= 20 nm). In order to correct multiple detections coming from the same pDendra2 molecule (Specht et al., 2013), we identified detections occurring in the vicinity of space (2 x sigma) and time (15 s) as belonging to a same molecule. The surface of gephyrin clusters and the densities of gephyrin molecules per μm^2 were measured in reconstructed 2D images through cluster segmentation based on detection densities. The threshold to define the border was set to 1000 detections/μm^2, taking into account the reported gephyrin densities in synapses (Specht et al, 2013; Fig. 3B). Briefly, all pixels (PALM pixel size=20 nm) containing less than 2 detections where considered as empty, and their intensity value set to zero. The intensity of pixels with at least two detections was set to one. The resulting binary image was analyzed with the function regionprops of Matlab (The Mathworks) to extract the surface area of each cluster identified by this function. Density was calculated as the total number of detections in the pixels belonging to a given cluster, divided the area of the cluster.

Statistics

Sampling corresponds to the number of quantum dots for SPT, the number of cells for ICC, and the number of synapses for PALM. Sample size selection for experiments was based on published experiments, pilot studies as well as in-house expertise. All results were used for analysis except in few cases. Cells with signs of suffering (apparition of blobs, fragmented neurites) were discarded from the analysis. Means are shown ± SEM, median values are indicated with their interquartile range (IQR, 25-75%). Means were compared using the non-parametric Mann-Whitney test (immunocytochemistry, dwell time comparison, PALM quantifications) using SigmaPlot 12.5 software (Systat Software). Diffusion coefficient and explored area values having non-normal distributions, a non-parametric Kolmogorov-Smirnov test was run under Matlab (The Mathworks, Natick, MA). Differences were considered significant for p-values less than 5% *(*$p \leq 0.05$; **$p < 0.01$; ***$p < 0.001$).*

Results:

eGFP-gephyrin mutants exhibit different clustering properties in culture.

Signaling pathways that converge onto gephyrin scaffolding properties influence $GABA_AR$ synaptic transmission. Hence, mimicking phosphorylation/ dephosphorylation events that influence gephyrin clustering can help gain critical insights into nanoscale regulation of $GABA_ARs$ at synaptic sites. ERK1/2 phosphorylation at the S268 residue results in smaller gephyrin clusters (Tyagarajan et al., 2013); hence, we selected phospho-mimetic eGFP-gephyrin-S268E mutant to study the impact of smaller clusters on receptor diffusion. Similarly, pharmacological blockade of the GSK3β pathway or eGFP-gephyrin-S270A mutant expression

increases gephyrin cluster number and size (Tyagarajan et al., 2011). We selected the eGFP-S270A mutant to understand how larger clusters would impact receptor diffusion. eGFP-gephyrin dominant negative (DN) mutant in primary neurons not only abolishes gephyrin clustering, reduces surface expression of $GABA_ARs$, but also significantly decreases GABAergic mIPSC amplitude and frequency (Ghosh et al., 2016). Hence, we selected eGFP-DN mutant to evaluate how cluster disruption would impact synaptic anchoring and surface diffusion of $GABA_ARs$.

Primary hippocampal neurons were co-transfected at 14 days *in vitro* (DIV) with eGFP-gephyrin WT (eGFP-WT), eGFP-S268E, eGFP-S270A or eGFP-DN along with shRNA targeting the gephyrin 3'UTR (to minimize the influence of endogenous gephyrin expression on mutant phenotypes). Before studying the influence of altered gephyrin clustering on $GABA_AR$ diffusion properties we first confirmed the respective gephyrin mutant morphology 6-9 days post-transfection. Representative images of neurons expressing either eGFP-WT or eGFP-S268E, eGFP-S270A, eGFP-DN variants are shown (Fig. 1A). We stained for the α2 $GABA_AR$ subunit to study the relation of eGFP-gephyrin with receptors. Quantification for eGFP-gephyrin cluster density (Nb), cluster size (area) and intensity (Int) showed a tendency for reduced clustering for the S268E mutant, and increased clustering for the S270A mutant (Fig 1B). The impact of the gephyrin S270A mutation on gephyrin cluster area and intensity was more pronounced, in comparison to S268E mutant. As expected eGFP-DN failed to cluster (data not shown). Similar to the observed changes in eGFP-gephyrin morphology, quantification of cluster intensity for α2 $GABA_AR$ showed a significant increase in neurons expressing eGFP-S270A, while eGFP-S268E expressing neurons only showed a modest reduction in α2 (Fig. 1C). The neurons expressing eGFP-DN showed very little α2 $GABA_AR$ staining (data not shown).

Influence of eGFP-gephyrin mutants on $GABA_AR$ surface diffusion.

$GABA_ARs$ are known to exhibit faster mobility at extrasynaptic sites as compared with synaptic sites. Due to their interaction with the main scaffolding molecule gephyrin $GABA_ARs$ are slowed down and confined at synapses. This diffusion-capture of $GABA_ARs$ is modulated by neuronal activity and constitutes an important basis for synaptic plasticity (ref in (Petrini and Barberis, 2014)). The expression of specific eGFP-gephyrin mutation allows us to lock the scaffold into different conformations and study its influence on $GABA_AR$ surface diffusion. To achieve this we assessed the lateral mobility of α2 $GABA_AR$ using quantum-dot (QD) based single particle tracking (QD-SPT). Live imaging over 600 constitutive frames at 75 Hz was used to record individual trajectories, and the trajectories were later analyzed using custom software (Fig. 2A) (see Material and Methods). As a proof of concept we first tested the effect of total gephyrin cluster removal on α2 $GABA_AR$ surface dynamics by expressing the eGFP-DN mutant. However, given that eGFP-DN has a diffuse expression, to distinguish synaptic and extra-synaptic α2 clusters we pre-loaded presynaptic GABAergic terminals using VGAT-Oyster550 antibody. The expression of the eGFP-DN mutant increased the surface exploration of QDs at both extrasynaptic and synaptic sites compared with control eGFP-WT. Quantification of the α2 $GABA_AR$ diffusion coefficient showed a 1.4 fold increase for extrasynaptic receptors and 1.2 fold increase for synaptic receptors in eGFP-DN expressing neurons (Fig. 2B). Area explored by α2 $GABA_ARs$ also showed a 1.6 fold increase at extrasynaptic sites and a 1.3 fold increase at synaptic sites in eGFP-DN expressing neurons (Fig. 2C). These observations support the notion that gephyrin not only slows down and confines $GABA_ARs$ at synapses but also at extrasynaptic sites (Ehrensperger et al., 2007).

Synaptic dwell time values can be discriminated from “trapped” receptors (dwell time>5.9 s) and “passing” receptors (dwell time<=5.9 s) (Renner et al., 2012). Quantification of α2 $GABA_AR$ dwell time confirmed a 1.3 fold faster escape time of receptors in neurons expressing the eGFP-DN mutant (Fig. 2D). We did not observe any difference in this rate for passing receptors. This is an indication that the observed reduction of trapped receptors is not due to increased membrane viscosity, but rather due to gephyrin scaffold’s influence on $GABA_AR$ surface mobility. Thus, we concluded that the diffuse DN gephyrin relieved $GABA_AR$ α2 diffusion constraints leading to synaptic escape of receptors.

If indeed gephyrin clustering can influence receptor diffusion, then S268E and S270A modification(s) must have an influence on α2 $GABA_AR$ surface mobility. To test this, we transfected the eGFP-S268E or eGFP-S270A mutants and measured surface mobility at extrasynaptic and synaptic locations. Superimposition of trajectories with fluorescent image of eGFP-gephyrin allowed us to distinguish synaptic versus extrasynaptic α2 $GABA_ARs$. Neurons transfected with eGFP-S268E exhibited an increase in surface exploration of individual trajectories (Fig. 2A). This was consistent with the observed increase in diffusion coefficients at both extrasynaptic and synaptic sites (Fig. 2E). Similarly, quantification of explored area at both extrasynaptic and synaptic sites showed significant increases (Fig. 2F). If reducing gephyrin cluster size facilitates α2 diffusion, then we expect shorter dwell time at synaptic sites. Indeed, we report reduced dwell time for trapped α2 $GABA_ARs$ in eGFP-S268E transfected neurons (Fig. 2G). Therefore the use of eGFP-S268E gephyrin mutant shows that the reduction in gephyrin cluster size causes increase in $GABA_AR$ diffusion, while reducing synaptic dwell time.

On the other hand, in eGFP-S270A transfected neurons, the α2 $GABA_A$Rs showed increased surface exploration of individual trajectories at synapses (Fig. 2A). Unexpectedly, diffusion coefficients and surface exploration of α2 extrasynaptic and synaptic $GABA_A$Rs were significantly increased in eGFP-S270A transfected neurons (Fig. 2E-F). However, analysis showed no reduction in α2 $GABA_A$R dwell time at synaptic sites (Fig. 2G). We thus concluded that the increase in receptor mobility at synapses in S270A transfected neurons does not correlate with what we may expect from a larger scaffold, suggesting additional regulations are at play.

Super-resolution PALM microscopy reveals differential packing of gephyrin scaffold.

We turned to quantitative nanoscopic imaging to understand the influence of phosphorylation on gephyrin scaffold organization. Using photoactivated localization microscopy (PALM) we estimated localization accuracy from several detections of the same fluorophore from subsequent image frames (Specht et al., 2013). The spatial resolution of PALM is within the range of ~25-30 nm; hence, image segmentation of the rendered PALM images can resolve substructure organization within a gephyrin cluster, that are not discernable using diffraction limited imaging (Specht et al., 2013). Employing fluorescence imaging on primary hippocampal neurons co-transfected with photo-convertible pDendra2-WT, pDendra2-S268E or pDendra2-S270A and shRNA 3'UTR showed a clustering phenotype consistent with eGFP-gephyrin and its mutant variants (Fig. 3A). PALM image cluster segmentation was established based on local density of detections using a threshold of 1000 detections/ μm^2 (Fig. 3B). Image segmentation allows us to estimate the mean surface area of a given pDendra2-WT cluster. In this case quantification showed pDendra2-WT clusters to be 0.054 ±

0.003μm^2, corresponding to the mean diameter of 262 nm as has been reported earlier (Specht et al., 2013). pDendra2-S268E quantifications showed a significant reduction in mean surface area to 0.035 ± 0.002 μm^2, and consistent with our expectations, pDendra2-S270A showed an increase in cluster area of 0.078 ± 0.005 μm^2 as expected (Fig. 3C).

We next tried to correlate the estimated size of gephyrin clusters to their respective densities. Our analysis showed 3919.7 ± 227.9 molecules/ μm^2 of pDendra2-WT molecules within a cluster (Fig. 3D). pDendra2-S268E showed a significantly increased molecular density (4457.5 ± 221.6) in spite of having a smaller cluster area. In contrast, pDendra2-S270A mutant shows a significantly reduced molecular density (2819.8 ± 117.6), in spite of having a larger surface area (Fig. 3D).

Our data indicate that there is no correlation between the diffusion properties of $GABA_A$Rs in spite of the relative size difference between S268E and S270A gephyrin clusters. However, there is a strong correlation between gephyrin phosphorylation and cluster microdomain compaction. The compaction of the scaffold or the increased spacing between gephyrin molecules may perturb the organization of the gephyrin microdomain thereby altering gephyrin-receptor binding properties. We cannot exclude the possibility that the mutations impact directly receptor-binding properties independently of their effect on the mesh.

Prolonged neuronal activity influences gephyrin and $GABA_A$R clustering as well as $GABA_A$R diffusion.

Activity-dependent regulation of receptor lateral diffusion is an essential contributor to synapse adaptation (Lüscher et al., 2011). This phenomenon has been explored within the experimental paradigm of short-term (1-60 min) drug applications (Bannai et al.,

2009; Muir et al., 2010; Niwa et al., 2012; Petrini et al., 2014; Bannai et al., 2015). There is accumulating evidence that synaptic adaptations at GABAergic synapses also occur in response to prolonged changes in activity (Rannals and Kapur, 2011; Vlachos et al., 2013; Flores et al., 2015). Hence, we examined whether gephyrin phosphorylation regulates activity-dependent membrane diffusion and synaptic recruitment of α2 $GABA_A$Rs. To test this hypothesis, we chronically elevated synaptic activity by treating our primary hippocampal neurons with the potassium channel blocker 4-aminopyridine (4-AP; 100 μM) (Chamma et al., 2013) for 8 h or 48 h. We used immunocytochemistry to determine the impact of a prolonged activity increase on gephyrin and α2 $GABA_A$R clustering (Fig. 4A). Quantification across independent experiments showed that fluorescence intensity of eGFP-WT gephyrin clusters increased by 1.95 fold after 8 h and by 2.3 fold after 48 h of 4-AP treatment (Fig. 4B). Quantification for α2 $GABA_A$R cluster intensity after 8 h of 4-AP induced neuronal activity did not show an increase in receptor accumulation at synapses; however, after 48 h of 4-AP treatment we found a 1.7 fold increase in receptor density at synaptic sites (Fig. 4C). Thus, gephyrin recruitment at synapses precedes that of the receptor in response to chronic changes in activity. In contrast to synaptic clusters, extrasynaptic α2 clusters decreased in size and intensity after 8 h of 4-AP application (Fig. 4D). This transient decrease in extrasynaptic α2 clusters intensity is reversed after 48 h of 4-AP similar to synaptic receptor clusters (Fig. 4C-D). Therefore, a chronic increase in activity regulates both extrasynaptic and synaptic receptor clustering.

It has been reported that acute 4-AP treatment increases $GABA_A$R mobility between synaptic and extrasynaptic sites (Bannai et al., 2009). Hence, we analyzed α2 $GABA_A$R surface diffusion at extrasynaptic and synaptic sites after either 8 h or 48 h of 4-AP treatment using QD-SPT (Fig. 4E). Quantification of the receptor diffusion coefficient

showed a 1.3 fold reduction for extrasynaptic receptors; however, the synaptic receptors were not influenced by 8 h of 4-AP treatment (Fig. 4F). Consistently, 8 h of 4-AP treatment reduced the explored area for only the extrasynaptic receptors by 1.2 fold (Fig. 4G). The receptor dwell time at synaptic sites was also unchanged after 8 h of activity change (Fig. 4H). This is consistent with a lack of receptor accumulation at synapses after 8 h of 4-AP treatment.

Contrary to the 8 h 4-AP treatment, 48 h treatment significantly reduced the diffusion coefficients of synaptic α2 receptors by 1.3 fold, while having no effect on the extrasynaptic receptors (Fig. 4I). We also observed a 1.3 fold reduction in explored area for synaptic α2 $GABA_A$Rs, with only a modest reduction for extrasynaptic receptors (Fig. 4J). Unexpectedly, the reduction in the diffusion rate and explored area of synaptic α2 receptors had no influence on the dwell time at synaptic sites (Fig. 4K). Therefore, pools of extrasynaptic and synaptic receptor are regulated independently of each other over prolonged activity change.

Altogether, our data show that $GABA_A$R lateral diffusion can be regulated on a time scale of days. We observe a decrease in synaptic $GABA_A$R diffusion at 48 h time point and not at 8 h, which is in direct correlation to cluster intensity change observed after 48 h. Therefore, regulation of $GABA_A$R diffusion capture accounts for the change in receptor density at synapses upon chronic changes in activity.

PKA and CaMKIIα pathways regulate synaptic scaling at GABAergic postsynaptic sites through gephyrin phosphorylation.

To identify signaling cascades which couple the gephyrin scaffold to $GABA_A$Rs for activity-dependent synaptic recruitment, we focused on the PKA and CaMKIIα pathways. NMDA receptor dependent compensatory adaptations at the GABAergic

postsynaptic sites have been reported to be facilitated by gephyrin phosphorylation at PKA and CaMKIIα locations (Flores et al., 2015). We thus transfected the eGFP-S303A/S305A (SSA) mutant (insensitive to PKA and CaMKIIα dependent phosphorylation) into our primary hippocampal neurons and treated the neurons for 8h or 48h with 4-AP. We did not observe differences between eGFP-WT and eGFP-SSA cluster number, cluster size and fluorescence intensity in control conditions (Fig. 5B). Similarly, the SSA mutant did not significantly influence the synaptic or extrasynaptic clustering of α2 $GABA_A$Rs (Fig. 5B). In contrast, the SSA mutation increased the diffusion coefficient and explored area of α2 $GABA_A$Rs at both extrasynaptic and synaptic sites (Fig. 5C-D). This increase in receptor mobility did not correlate with what we expected from a normal size scaffold. However, the α2 $GABA_A$Rs dwell time at inhibitory synapses did not differ between eGFP-SSA and eGFP-WT transfected neurons (Fig. 5E), indicating that the increase in receptor mobility was not accompanied by a faster synaptic escape of receptors. This is consistent with a lack of effect of the SSA mutant on α2 $GABA_A$Rs clustering at synapses.

The expression of the eGFP-SSA mutant was sufficient to prevent the 4-AP (8 h or 48 h) induced gephyrin and α2 $GABA_A$Rs cluster growth at synapses (Fig. 5A, F-G). Interestingly, 8 h and 48 h post 4-AP application extrasynaptic α2 cluster intensity increased in eGFP-SSA transfected neurons (Fig. 5H). This indicated that receptor clustering at extrasynaptic sites at the 8 h treatment time point is dependent on PKA and CaMKIIα phosphorylation. However, at 48 h receptor accumulation is independent of these two pathways. Hence, an additional pathway permits $GABA_A$R recruitment, in particular at extrasynaptic sites, after chronic changes in activity.

We also analyzed the effect of the SSA mutant on α2 $GABA_A$Rs surface diffusion. Similar to wild-type gephyrin, SSA reduced diffusion coefficient and surface

exploration of α2 $GABA_A$Rs at extrasynaptic sites after 8 h of 4-AP (Fig. 5I-J). This effect was maintained also after 48 h treatment (Fig. 5K-L). In contrast to wild-type gephyrin, SSA mutant increased α2 $GABA_A$R confinement, and decreased resident time of $GABA_A$Rs at synapses after 48 h of 4-AP (Fig. 5K-M). The passing α2 $GABA_A$Rs remained unchanged at synapses after 8 h or 48 h of 4-AP (Fig. 5M). Hence, our results indicate that gephyrin scaffold reorganization via PKA and CaMKIIα dependent phosphorylation at S303 and S305 is essential for $GABA_A$R diffusion at synapses but not at extrasynaptic sites in response to chronic changes in activity.

Synapse scaling is independent of ERK1/2 pathway.

It has been reported that gephyrin clustering is also influenced by ERK1/2 pathway. We thus assessed if ERK1/2 signaling influences gephyrin cluster size during chronic changes in network activity. Transgenic expression of eGFP-S268E gephyrin mutant renders gephyrin scaffold insensitive to the ERK1/2 signaling pathway (Tyagarajan et al., 2013). We therefore transfected cultured neurons with eGFP-S268E mutant and treated them with 4-AP for 8 h or 48 h. Immunocytochemical analysis showed an increase in eGFP-S268E mutant cluster size after 4-AP treatment (Fig. 6A). Quantification of changes in eGFP-S268E cluster intensity confirmed an increase of 1.6 and 2.2 fold after 8 h and 48 h of 4-AP treatment respectively (Fig. 6B). This was associated with increases of 1.2 and 1.3 fold in eGFP-S268E cluster size after 8 h and 48 h of 4-AP treatment respectively (Fig. 6B). Analysis for α2 $GABA_A$R cluster intensity at synapses and at extrasynaptic sites showed a respective 2.2 and 1.8 fold increase after 48 h of 4-AP treatment, but not after 8 h (Fig. 6C-D). We conclude that the eGFP-S268E mutant is not required for the activity-dependent recruitment of gephyrin and $GABA_A$R within synaptic and extrasynaptic clusters. We wondered if 4-

AP induced chronic activity would impact the surface diffusion of $GABA_A$Rs. We checked α2 $GABA_A$R diffusion coefficients after 8 h or 48 h of 4-AP. Individual receptor trajectories for extrasynaptic and synaptic α2 $GABA_A$R suggested increased confinement after 48 h of enhanced activity (Fig. 6E). The α2 diffusion coefficients and explored area were increased by 1.2 fold and 1.4 fold for extrasynaptic receptors after 8 h of 4-AP (Fig. 6F-G). However, 48 h post 4-AP application extrasynaptic receptors diffusion coefficients were unchanged (Fig 6H), while QDs were more confined at extrasynaptic sites (Fig. 6I). Interestingly, 48 h of 4-AP treatment reduced synaptic α2 $GABA_A$R diffusion coefficients and explored area at eGFP-S268E synapses (Fig. 6H-I) as observed at synapses containing eGFP-WT (Fig. 4I-J). In agreement with an increased number of α2 $GABA_A$Rs at synapses, α2 dwell time increased at eGFP-S268E synapses (Fig. 6J).

Therefore, we conclude that although ERK1/2 signaling is not necessary for the activity-dependent regulation of the diffusive behavior of synaptic $GABA_A$Rs, it controls the mobility of receptors at extrasynaptic sites. These observations further confirm that synaptic and extrasynaptic receptor pools are independently regulated, and that adaptations observed at GABAergic postsynapses is independent of ERK1/2 pathway.

GSK3β phosphylation of gephyrin facilitates $GABA_A$R diffusion after activity change.

It has been reported that the GSK3β signaling pathway postsynaptically regulates the density and size of GABAergic synapses via gephyrin phosphorylation. Pharmacological blockade of the GSK3β pathway or expression of the S270A gephyrin mutant is sufficient to increase gephyrin cluster size (Tyagarajan et al., 2011). Hence,

it is plausible that GSK3β pathway acts in addition to PKA and CaMKIIα signaling to regulate homeostatic adaptations at GABAergic synapses. To address this question, we treated neurons transfected with eGFP-S270A gephyrin mutant with 4-AP for 8 h and 48 h. Morphological characterization showed that the GSK3β signaling is not essential for gephyrin accumulation at synapses upon chronic changes in activity (Fig. 7A-B). In contrast, the eGFP-S270A mutant fully abolished the synaptic and extrasynaptic increase in α2 $GABA_AR$ clustering after 48 h of 4-AP application (Fig. 7C-D). After 8h of 4-AP treatment extrasynaptic α2 $GABA_AR$ cluster density, size and intensity were respectively reduced by 1.4 fold, 1.2 fold and 1.4 fold in eGFP-S270A expressing cells, respectively (Fig. 7D). These results implicate the GSK3β pathway in the regulation of activity-induced $GABA_AR$ clustering at both synaptic and extrasynaptic sites.

If the GSK3β signaling is important for $GABA_ARs$ accumulation at synapses in response to chronic changes in activity, then eGFP-S270A mutant expression should have no impact on α2 diffusion rates. However, 8 h post 4-AP application α2 diffusion coefficient and explored area were reduced by 1.3 fold and 1.1 fold at synaptic sites (Fig. 7E-G). This increased confinement was counterbalanced by a decrease in the time trapped receptors spent at synapses (Fig. 7J), explaining why α2 clustering was unchanged at synapses after 8 h of 4-AP application. On the other hand, 48 h of 4-AP application increased α2 diffusion coefficients by 1.3 fold as well as explored area at synaptic sites (Fig. 7E, H-I). This was however not accompanied by a change in synaptic receptor dwell time (Fig. 7J). The reduction of extrasynaptic α2 clustering coincided with a 1.3 fold reduced explored area in eGFP-S270A expressing cells after 8 h of 4-AP (Fig. 7E-G). Nevertheless, 48 h after 4-AP application α2 diffusion coefficients and explored area returned to baseline levels at extrasynaptic sites (Fig.

7H-I). These observations are consistent with the receptor clustering returning to control levels at extrasynaptic sites after 48 h of 4-AP (Fig. 7D). Altogether, these results show that GSK3β signaling in addition to PKA and CaMKIIα pathways tune $GABA_A$Rs at synapses in response to chronic changes in activity.

Impairment of PKA, CAMKIIα and GSK3β phosphylation of gephyrin abolishes the activity-dependent regulation of $GABA_A$Rs mobility.

The analysis of the SSA and S270A mutants indicated that PKA, CAMKIIα and GSK3β phosphylation of gephyrin have complementary effects on gephyrin and α2 $GABA_A$Rs clustering in conditions of synaptic plasticity. To show it more directly, we generated eGFP-SSA/S270A mutant, expressed it in hippocampal neurons and treated the neurons for 8 h or 48 h with 4-AP.

We found that overexpressing eGFP-SSA/S270A increased eGFP cluster size and intensity (Fig. 8A). The gephyrin cluster growth was however not accompanied by synaptic recruitment of α2 $GABA_A$Rs (Fig. 8A). Although the density of α2 $GABA_A$Rs clusters was reduced in eGFP-SSA/S270A transfected cells, there was no major impact of the mutant on α2 $GABA_A$Rs cluster size and intensity at synaptic and extrasynaptic sites (Fig. 8A).

We then characterized α2 $GABA_A$R diffusion in SSA/S270A transfected neurons. Diffusion coefficients showed a 1.4 fold increase for extrasynaptic receptors and no significant change for synaptic receptors (Fig. 8B). This effect was consistent with the observation that α2 $GABA_A$R spent the same time at eGFP-SSA/S270A and eGFP-WT synapses (Fig. 8C). Therefore the eGFP-SSA/S270A mutant can recapitulate many of the observed phenotypes seen with SSA or S270A individual mutations.

We then characterized how chronic activity impacts eGFP-SSA/S270A mutant behavior. Although the extrasynaptic $GABA_A$Rs cluster density increased after 48 h of 4-AP in eGFP-SSA/S270A transfected cells, the triple mutant prevented the synaptic increase in gephyrin and $GABA_A$Rs cluster size and intensity in response to 4-AP treatment (Fig. 8D-F). The diffusion coefficient and explored area of α2 $GABA_A$Rs showed no change after 8 h or 48 h of 4-AP application (Fig. 8 G-J). There was also no impact on receptor dwell time at synapses after chronic changes in activity (Fig. 8K). Our results uncover a role for several signaling pathways in chronic activity-dependent modulation of gephyrin clustering and $GABA_A$Rs surface diffusion at synapses. Our data also show that distinct signaling pathways regulate synaptic and extrasynaptic receptors clustering. Together these results identify a novel role of GSK3β signaling in the regulation of extrasynaptic receptor surface trafficking and GSK3β, PKA and CaMKIIα pathways in facilitating adaptations of synaptic receptors.

Discussion:

In the current study, we investigate the molecular basis for gephyrin scaffold induced $GABA_A$R membrane dynamics. We identify a novel role for gephyrin post-translational modification involving phosphorylation and de-phosphorylation in regulating $GABA_A$R lateral diffusion. By tracking α2 $GABA_A$Rs within and outside synaptic sites using QD-SPT, we demonstrate that gephyrin phosphorylation by ERK1/2 at S268, and inhibition of GSK3β phosphorylation on gephyrin at S270 while exhibiting opposite effects on synaptic morphology, influence $GABA_A$R diffusion properties similarly. We analyze gephyrin scaffold organization at the nanoscale level using PALM, and uncover that phosphorylation also controls gephyrin molecule packing.

Over the past decade, several independent studies have documented changes in lateral diffusion of $GABA_AR$s after pharmacological alteration of neuronal function within a time scale of minutes to few hours (Lévi et al., 2008; Bannai et al., 2009; Niwa et al., 2012; Petrini et al., 2014). 4-AP application within minutes induces NMDAR-mediated calcium influx and calcineurin activation leading to dephosphorylation of the $GABA_AR$ γ2 subunit S327 residue (Wang et al., 2003). In this context, an increase in $GABA_AR$ diffusion constraint results from receptor dephosphorylation, while gephyrin scaffold loss is a secondary effect in response to receptor dispersal (Niwa et al., 2012). We identify gephyrin phosphorylation as an essential facilitator of $GABA_AR$ diffusion dynamics in response to chronic changes in activity. More specifically we identify a central role for PKA and CaMKIIα pathways along with GSK3β signaling in phosphorylating gephyrin to regulate activity-dependent inhibitory synapse remodeling.

Structure of the gephyrin scaffold requires phosphoregulation of gephyrin molecules.

At GABAergic synapses the role of phosphorylation for gephyrin scafigffold compaction have yet to be reported. The fluorescence microscopy data (Figure 1B) inform us about average area and intensity per cluster. PALM microscopy informs us about the actual density of molecules per surface area (Figure 3). The number of molecules per synapse using PALM imaging can be roughly estimated by multiplying the mean surface area of the cluster by the density of gephyrin molecules per surface unit. Values of ~ 212, 156 and 220 were found for the gephyrin WT, S268E and S270A respectively. Interestingly, these estimations are consistent with the measurements of the mean cluster fluorescence intensity for the S268E and S270A mutants.

The hexameric gephyrin lattice model was proposed based on G and E domain crystal structures available at the time. However, in recent years atomic force microscopy (AFM) and small-angle X-ray scattering (SAXS) structure of full-length gephyrin has shown that gephyrin only exist as trimers, as individual E domains are in an open extended confirmation (Sander et al., 2013). (Pennacchietti et al., 2017) have shown that after iLTP gephyrin reorganizes itself into distinct subsynaptic nanodomains. Full-length gephyrin can exist in open or closed confirmations based on the linker domain folding (Sander et al., 2013). All the gephyrin phosphorylation sites have been mapped to the linker domain suggesting phosphorylation is a strong candidate for determining open and closed states within gephyrin nanodomains. This could in turn determine the distance between two nanodomains and/or total number of nanodomains within a given synapse.

Gephyrin-independent $GABA_AR$ adaptations at synaptic sites.

It has long been assumed that alterations in $GABA_AR$ and/or gephyrin cluster intensity is indicative of the number of molecules found at the synapse, and thereby a direct correlate for changes in synapse structure and function. Here we report that disrupting gephyrin scaffold via the expression of the eGFP-DN mutant does not increase the diffusion properties of $GABA_ARs$ at synaptic sites. This observation was unexpected as loss of the scaffolding apparatus should have increased receptor diffusion also at synaptic sites. It has been reported that eGFP-DN expression significantly reduces mIPSC amplitude and frequency, without leading to a complete loss of GABAergic synaptic transmission (Ghosh et al., 2016). Our observation suggests that a pool of gephyrin independent $GABA_ARs$ are present in neurons. Recently, GIT1/βPIX/Rac1/PAK signaling pathway was shown to contribute to GABAergic

transmission. βPIX is a GEF for Rac1 activating PAK, and contributing to $GABA_AR$ stability (Smith et al., 2014). Similar signaling mechanisms could be operational even in the absence of gephyrin scaffold to maintain the membrane pool of $GABA_ARs$.

Independent behavior of $GABA_ARs$ at synaptic and extrasynaptic sites.

Postsynaptic receptor trapping is adaptable depending on phosphorylation events that impinge on scaffold-scaffold or receptor-scaffold interactions (Choquet and Triller, 2013). It became clear with the development of SPT approaches that receptors are also hindered in their diffusion outside synapses via molecular crowding but also through specific protein-protein interactions. A receptor-gephyrin interaction outside inhibitory synapses has been reported earlier (Ehrensperger et al., 2007). $GABA_ARs$ also colocalize and interact with clathrin-enriched endocytic zones (EZs) that are mostly localized extrasynaptically (Smith et al., 2012). Receptors in EZs don't necessarily undergo internalization. They can be part of a reserve pool of receptors rapidly available upon increase in synaptic activity (Petrini et al., 2014). Conversely, the $GABA_AR$-AP2 interaction within EZs has been shown to indirectly control receptor mobility and number at synapses (Smith et al., 2012).

However, our data show independent behavior of $GABA_ARs$ at synaptic and extrasynaptic sites. After 8 h of 4-AP treatment α2 $GABA_ARs$ were confined at extrasynaptic sites without influencing the diffusion property of synaptic receptors. In contrast, after 48 h of 4-AP treatment α2 $GABA_AR$ confinement at extrasynaptic sites was lifted, and this was followed by an increase in receptor confinement at synapses, suggesting that $GABA_AR$ retention at extrasynaptic sites prevent their synaptic capture/accumulation. However, after 8 h of 4-AP treatment neurons expressing eGFP-S268E mutant show a reduction in receptor confinement at extrasynaptic locations,

without affecting synaptic receptor diffusion. Therefore, removing diffusion constraints onto extrasynaptic $GABA_A$Rs does not facilitate receptor recruitment at synapses. In addition, after 8 h of 4-AP treatment neurons expressing eGFP-S270A mutant show increased confinement of $GABA_A$Rs at both extrasynaptic and synaptic locations, indicating that confining $GABA_A$Rs at extrasynaptic locations does not prevent diffusion-capture of receptors.

Synaptic adaptation is facilitated by gephyrin phosphorylation.

We present evidence for a biphasic model for activity-dependent plasticity at GABAergic postsynapse. Acute 4-AP treatment increases and chronic 4-AP treatment decreases α2 $GABA_A$R lateral diffusion. The observed increase in $GABA_A$R diffusion after acute 4-AP treatment can be explained by increase in synaptic escape of receptors leading to reduced postsynaptic clustering and dispersal of gephyrin molecules away from the synapse (Bannai et al., 2009). On the contrary, we show here that chronic 4-AP treatment leads to synaptic immobilization and recruitment of $GABA_A$R α2 and gephyrin. These discrepancies are probably due to the distinct signaling pathways activated by the acute and chronic changes in activity. Short term 4-AP application induces NMDAR-mediated calcium influx and calcineurin activation leading to dephosphorylation of $GABA_A$R γ2 subunit S327 residue (Bannai et al., 2009). In this context, the relief in $GABA_A$R diffusion constraints arises from receptor dephosphorylation while gephyrin loss is a consequence of receptor dispersal (Niwa et al. 2012). In contrast, we show that chronic changes in activity impacts first the recruitment of gephyrin at synapses, and then allows the recruitment of $GABA_A$Rs. PKA and CaMKIIα signaling act downstream of NMDAR to facilitate compensatory postsynaptic adaptations at GABAergic synapses (Flores et al., 2015). Our data extends

this understanding by demonstrating a role for the GSK3β pathway in addition to PKA and CaMKIIα pathways in facilitating gephyrin scaffold organization of individual $GABA_A$Rs after prolonged changes in activity.

References:

Bannai H, Lévi S, Schweizer C, Inoue T, Launey T, Racine V, Sibarita J-B, Mikoshiba K, Triller A (2009) Activity-dependent tuning of inhibitory neurotransmission based on GABAAR diffusion dynamics. Neuron 62:670–682.

Bannai H, Niwa F, Sherwood MW, Shrivastava AN, Arizono M, Miyamoto A, Sugiura K, Lévi S, Triller A, Mikoshiba K (2015) Bidirectional Control of Synaptic GABAAR Clustering by Glutamate and Calcium. Cell Rep 13:2768–2780.

Bats C, Groc L, Choquet D (2007) The interaction between Stargazin and PSD-95 regulates AMPA receptor surface trafficking. Neuron 53:719–734.

Chamma I, Heubl M, Chevy Q, Renner M, Moutkine I, Eugène E, Poncer JC, Lévi S (2013) Activity-dependent regulation of the K/Cl transporter KCC2 membrane diffusion, clustering, and function in hippocampal neurons. J Neurosci 33:15488–15503.

Charrier C, Machado P, Tweedie-Cullen RY, Rutishauser D, Mansuy IM, Triller A (2010) A crosstalk between β1 and β3 integrins controls glycine receptor and gephyrin trafficking at synapses. Nat Neurosci 13:1388–1395.

Chen JL, Villa KL, Cha JW, So PTC, Kubota Y, Nedivi E (2012) Clustered dynamics of inhibitory synapses and dendritic spines in the adult neocortex. Neuron 74:361–373.

Choquet D, Triller A (2013) The dynamic synapse. Neuron 80:691–703.

Ehrensperger M-V, Hanus C, Vannier C, Triller A, Dahan M (2007) Multiple association states between glycine receptors and gephyrin identified by SPT analysis. Biophysical Journal 92:3706–3718.

Flores CE, Nikonenko I, Mendez P, Fritschy J-M, Tyagarajan SK, Muller D (2015) Activity-dependent inhibitory synapse remodeling through gephyrin phosphorylation. Proceedings of the National Academy of Sciences 112:E65–E72.

Ghosh H, Auguadri L, Battaglia S, Simone Thirouin Z, Zemoura K, Messner S, Acuña MA, Wildner H, Yévenes GE, Dieter A, Kawasaki H, O Hottiger M, Zeilhofer HU, Fritschy J-M, Tyagarajan SK (2016) Several posttranslational modifications act in concert to regulate gephyrin scaffolding and GABAergic transmission. Nat Commun 7:13365.

Lardi-Studler B, Smolinsky B, Petitjean CM, Koenig F, Sidler C, Meier JC, Fritschy JM, Schwarz G (2007) Vertebrate-specific sequences in the gephyrin E-domain regulate cytosolic aggregation and postsynaptic clustering. J Cell Sci 120:1371–1382.

Lévi S, Schweizer C, Bannai H, Pascual O, Charrier C, Triller A (2008) Homeostatic regulation of synaptic GlyR numbers driven by lateral diffusion. Neuron 59:261–273.

Lüscher B, Fuchs T, Kilpatrick CL (2011) GABAA receptor trafficking-mediated plasticity of inhibitory synapses. Neuron 70:385–409.

Muir J, Arancibia-Carcamo IL, MacAskill AF, Smith KR, Griffin LD, Kittler JT (2010)

NMDA receptors regulate GABAA receptor lateral mobility and clustering at inhibitory synapses through serine 327 on the γ2 subunit. Proceedings of the National Academy of Sciences 107:16679–16684.

Niwa F, Bannai H, Arizono M, Fukatsu K, Triller A, Mikoshiba K (2012) Gephyrin-independent GABA(A)R mobility and clustering during plasticity. PLoS ONE 7:e36148.

Pennacchietti F, Vascon S, Nieus T, Rosillo C, Das S, Tyagarajan SK, Diaspro A, Del Bue A, Petrini EM, Barberis A, Cella Zanacchi F (2017) Nanoscale Molecular Reorganization of the Inhibitory Postsynaptic Density Is a Determinant of GABAergic Synaptic Potentiation. J Neurosci 37:1747–1756.

Petrini EM, Barberis A (2014) Diffusion dynamics of synaptic molecules during inhibitory postsynaptic plasticity. Front Cell Neurosci 8:300.

Petrini EM, Ravasenga T, Hausrat TJ, Iurilli G, Olcese U, Racine V, Sibarita J-B, Jacob TC, Moss SJ, Benfenati F, Medini P, Kneussel M, Barberis A (2014) Synaptic recruitment of gephyrin regulates surface GABAA receptor dynamics for the expression of inhibitory LTP. Nat Commun 5.

Rannals MD, Kapur J (2011) Homeostatic strengthening of inhibitory synapses is mediated by the accumulation of GABA(A) receptors. J Neurosci 31:17701–17712.

Renner M, Schweizer C, Bannai H, Triller A, Lévi S (2012) Diffusion Barriers Constrain Receptors at Synapses Tell F, ed. PLoS ONE 7:e43032.

Saliba RS, Michels G, Jacob TC, Pangalos MN, Moss SJ (2007) Activity-dependent

ubiquitination of GABA(A) receptors regulates their accumulation at synaptic sites. J Neurosci 27:13341–13351.

Sander B, Tria G, Shkumatov AV, Kim EY, Grossmann JG, Tessmer I, Svergun DI, Schindelin H (2013) Structural characterization of gephyrin by AFM and SAXS reveals a mixture of compact and extended states. Acta Crystallogr D Biol Crystallogr 69:2050–2060.

Smith KR, Davenport EC, Wei J, Li X, Pathania M, Vaccaro V, Yan Z, Kittler JT (2014) GIT1 and βPIX are essential for GABA(A) receptor synaptic stability and inhibitory neurotransmission. Cell Rep 9:298–310.

Smith KR, Muir J, Rao Y, Browarski M, Gruenig MC, Sheehan DF, Haucke V, Kittler JT (2012) Stabilization of GABA(A) receptors at endocytic zones is mediated by an AP2 binding motif within the GABA(A) receptor β3 subunit. J Neurosci 32:2485–2498.

Specht CG, Izeddin I, Rodriguez PC, Beheiry El M, Rostaing P, Darzacq X, Dahan M, Triller A (2013) Quantitative nanoscopy of inhibitory synapses: counting gephyrin molecules and receptor binding sites. Neuron 79:308–321.

Tyagarajan SK, Ghosh H, Yévenes GE, Imanishi SY, Zeilhofer HU, Gerrits B, Fritschy J-M (2013) Extracellular signal-regulated kinase and glycogen synthase kinase 3β regulate gephyrin postsynaptic aggregation and GABAergic synaptic function in a calpain-dependent mechanism. J Biol Chem 288:9634–9647.

Tyagarajan SK, Ghosh H, Yévenes GE, Nikonenko I, Ebeling C, Schwerdel C, Sidler C, Zeilhofer HU, Gerrits B, Muller D, Fritschy J-M (2011) Regulation of GABAergic synapse formation and plasticity by GSK3beta-dependent

phosphorylation of gephyrin. Proceedings of the National Academy of Sciences 108:379–384.

van Versendaal D, Rajendran R, Saiepour MH, Klooster J, Smit-Rigter L, Sommeijer J-P, De Zeeuw CI, Hofer SB, Heimel JA, Levelt CN (2012) Elimination of Inhibitory Synapses Is a Major Component of Adult Ocular Dominance Plasticity. Neuron 74:374–383.

Villa KL, Berry KP, Subramanian J, Cha JW, Oh WC, Kwon H-B, Kubota Y, So PTC, Nedivi E (2016) Inhibitory Synapses Are Repeatedly Assembled and Removed at Persistent Sites In Vivo. Neuron 89:756–769.

Vlachos A, Reddy-Alla S, Papadopoulos T, Deller T, Betz H (2013) Homeostatic regulation of gephyrin scaffolds and synaptic strength at mature hippocampal GABAergic postsynapses. Cereb Cortex 23:2700–2711.

Wang J, Liu S, Haditsch U, Tu W, Cochrane K, Ahmadian G, Tran L, Paw J, Wang Y, Mansuy I, Salter MM, Lu YM (2003) Interaction of calcineurin and type-A GABA receptor gamma 2 subunits produces long-term depression at CA1 inhibitory synapses. J Neurosci 23:826–836.

Yu W, Jiang M, Miralles CP, Li R-W, Chen G, De Blas AL (2007) Gephyrin clustering is required for the stability of GABAergic synapses. Mol Cell Neurosci 36:484–500.

Figure Legends

Figure 1: Morphological characterization of eGFP-gephyrin and its mutant variants. (A) Representative images of primary hippocampal neurons co-transfected with eGFP-WT, eGFP-S268E, eGFP-S270A or eGFP-DN and shRNA-3'UTR. eGFP-gephyrin cluters (green), α2 $GABA_A$Rs (red) and VGAT (blue) are shown. Scale bar, 10 μm. **(B)** Quantification of eGFP-gephyrin cluster density, cluster area and intensity shows larger eGFP-S270A clusters compared with eGFP-WT at synapses. **S268E**: WT n= 66 cells, S268E n= 60 cells, 4 cultures. **Syn**: Cluster Number (Nb) p= 0.42, area p= 0.22, intensity (Int) p= 0.05. **Extra**: Nb p= 0.99, Area p= 0.66, Intensity p= 0.44. S270A: WT n= 86 cells, **S270A:** n= 74 cells, 6 cultures. **Syn**: Nb p= 0.77, Area p= 0.02, Intensity p= 0.02. **Extra**: Nb p= 0.39, Area p= 0.42, Intensity p= 0.15. **(C)** Quantification for α2 $GABA_A$R clusters shows significantly more receptors in eGFP-S270A mutant clusters. **S268E**: WT n= 52 cells, S268E n= 47 cells, 3 cultures. **Syn**: Nb p= 0.48, Area p= 0.46, Intensity p= 0.6. **Extra**: Nb p= 0.46, area p= 0.63, intensity p= 0.22. **S270A**: WT n= 52 cells, S270A n= 39 cells, 3 cultures. **Syn**: Nb p= 0.56, Area p= 0.08, Intensity p= 0.008. **Extra**: Nb p= 0.008, Area p= 0.81, Intensity p= 0.29. Data shown as mean ± SEM. Values were normalized to the corresponding control values. Statistics *P≤0.05, **P≤0.01 (Mann Whitney Rank sum test).

Figure 2: Membrane dynamics of α2 $GABA_A$R is influenced by gephyrin phosphorylation. (**A)** Example traces of QD trajectories (red) overlaid with fluorescent synaptic clusters (white) of VGAT-Oyster550 for eGFP-DN transfected neurons or with eGFP-gephyrin clusters for eGFP-WT, eGFP-S268E or eGFP-S270A expressing cells. Scale bar, 0.5 μm. (**B**) Median diffusion coefficients D of α2 $GABA_A$R in neurons transfected with either eGFP-WT or eGFP-DN. **Extra**: WT n= 975 QDs, DN n= 491

QDs, p= 4.5 10^{-34}; **Syn**: WT n= 306 QDs, DN n= 173 QDs, p= 0.36. **(C)** Quantification of explored area EA of α2 $GABA_AR$, **Extra**: WT n= 2925 QDs, DN n= 1473 QDs, p= 3.8 10^{-23}; **Syn**: WT n= 918 QDs, DN n= 519 QDs, p= 4.4 10^{-4}. **(D)** Dwell time DT of α2 $GABA_AR$ at synapses in neurons transfected with either eGFP-WT or eGFP-DN. Quantification of all QDs (total), trapped (DT < 5.9 s) and passing (DT > 5.9 s) QDs at inhibitory synapses. Significant decrease in synaptic dwell time for total and trapped QDs was observed but not for passing ones. **Total**: WT n= 436 QDs, DN n= 262 QDs, p= 0.001; **Trapped**: WT n= 235 QDs, DN n= 108 QDs, p= 8.0 10^{-3}; **Passing**: WT n= 201 QDs, DN n= 154 QDs, p= 0.19. **(E)** Quantification of diffusion coefficients of α2 $GABA_AR$ showing increased receptor mobility at extrasynaptic (extra) and synaptic (syn) sites in neurons transfected with eGFP-S268E or eGFP-S270A, as compared with eGFP-WT expressing cells. **Extra**: WT n= 1820 QDs, S268E n= 1273 QDs, p= 1.1 10^{-22}, S270A n= 1658, p= 2.9 10^{-27}. **Syn**: WT n= 461 QDs, S268E n= 326 QDs, p= 2.4 10^{-8}, S270A n= 340, p= 1.8 10^{-8}. (**F**) Quantification of α2 $GABA_AR$ explored area EA, **Extra**: WT n= 5460 QDs, S268E n= 3807 QDs, p=6.8 10^{-52}, S270A n= 5355, p= 2.2 10^{-101}. **Syn**: WT n= 1383 QDs, S268E n= 978 QDs, p= 7.4 10^{-23}, S270A n= 2208, p= 1.2 10^{-33}. **(G)** Quantification of α2 $GABA_AR$ dwell time DT in neurons expressing either eGFP-WT, eGFP-S268E or eGFP-S270A. Calculations were done for all QDs (total), (trapped) or (passing) QDs at inhibitory synapses. Decrease in dwell time for the whole or trapped population of QDs was seen in synapses expressing eGFP-S268E but not in synapses containing eGFP-S270A. **Total**: WT n= 251 QDs, S268E n= 176 QDs, p= 0.013, S270A n= 216 QDs, p= 0.31; **Trapped**: WT n= 135 QDs, S268E n= 85 QDs, p= 0.002, S270A n= 109 QDs, p= 0.28; **Passing**: WT n= 116 QDs, S268E n= 91 QDs, p= 0.24, S270A n= 107 QDs, p= 0.98. All data are from six independent experiments. In B-C, E-F, data are presented as median values ± 25%-75% Interquartile

Range IQR, ***P≤0.001 (Kolmogorov-Smirnov test). In D, G, data are presented as mean ± SEM. *P≤0.05, **P≤0.01 (Mann Whitney Rank sum test). D in $\mu m^2 s^{-1}$, EA in μm^2, DT in s.

Figure 3: PALM imaging showing gephyrin phosphorylation influences scaffold packing. (A) Epifluorescence (top) and PALM (bottom) imaging of the same dendritic regions in neurons expressing pDendra2-WT, -S268E or -S270A mutant. Scale bar, 1 µm. **(B)** Representative image of cluster segmentation (red) based on local density of molecules detected (white dots) using a threshold of 1000 detections/μm^2 (blue). Scale bar, 200 nm. **(C)** Quantification of eGFP cluster area using PALM shows reduction in cluster size for eGFP-S268E and increase in cluster size for eGFP-S270A compared with eGFP-WT. WT n= 313 synapses, S268E n= 277 synapses, S270A n= 290 synapses, p<0.001, 4 cultures. (**D**) Quantification of density of gephyrin molecules per μm^2 using PALM in transfected neurons. Neurons expressing eGFP-S268E exhibit denser gephyrin packing, and neurons expressing eGFP-S270A exhibit less dense packing of gephyrin compared with eGFP-WT. Data are presented as mean ± SEM. **P= 0.006; ***P≤0.001 (Mann Whitney Rank sum test).

Figure 4: Gephyrin clustering influences $GABA_AR$ lateral diffusion. (A) Morphology of eGFP-WT (green) after 8 h and 48 h of 4-AP application; VGAT (blue), $GABA_AR$ α2 (red) at 21 DIV. Scale bar, 10 µm. **(B)** Quantification of eGFP-WT clusters after 8 h and 48 h of 4-AP application. t0 n= 55 cells, 8h n= 46 cells, 48h n= 55 cells, 3 cultures. **Cluster Nb**: 0-8h: p= 0.13, 0-48h: p= 0.002; **Area**: 0-8h: p= 0.5, 0-48h: p= 0.001; **Intensity**: 0-8h: p<0.001, 0-48h: p<0.001. **(C)** Quantification of synaptic α2 $GABA_AR$ clusters after 8 h and 48 h of 4-AP compared with mock treated

control. t0 n= 52 cells, 8h n= 43 cells, 48h n= 53 cells, 3 cultures. **Cluster Nb**: 0-8h: p= 0.4, 0-48h: p= 0.3; **Area**: 0-8h: p= 0.8, 0-48h: p= 0.8; **Intensity**: 0-8h: p= 0.5, 0-48h: p= 0.03. **(D)** Quantification of extrasynaptic α2 $GABA_AR$ clusters after 8 h and 48 h of 4-AP compared with mock treated control. t0 n= 52 cells, 8h n= 43 cells, 48h n= 53 cells, 3 cultures. **Cluster Nb**: 0-8h: p= 0.2, 0-48h: p= 0.9; **Area**: 0-8h: p= 0.02, 0-48h: p= 0.3; **Intensity**: 0-8h: p= 0.05, 0-48h: p= 0.022. (**E)** Example trace of α2 $GABA_AR$ trajectories showing surface exploration of extrasynaptic and synaptic receptors after 8 h and 48 h of 4-AP exposure. Scale bar, 0.5 µm. (**F)** Quantification of diffusion coefficients of α2 $GABA_AR$ after 8 h of 4-AP exposure. **Extra**; t0 n= 450 QDs, WT 4AP 8h n= 961 QDs, p= $1.96\ 10^{-7}$. **Syn**; t0 n= 103 QDs, 8h n= 138 QDs, p= 0.22; 2 cultures. (**G)** Quantification of explored area EA of α2 $GABA_AR$ after 8 h of 4-AP application. **Extra**; t0 n= 1347 QDs, 8h n= 5265 QDs, p= $6.4\ 10^{-9}$. **Syn**; t0 n= 308 QDs, 8h n= 708 QDs, p= 0.63. **(H)** Quantification of synaptic dwell time DT of α2 $GABA_AR$ showing no impact after 8 h of 4-AP for either total, trapped or passing receptor population. **Total**: t0 n= 151 QDs, 8h n= 206 QDs, p= 0.073; **Trapped**: t0 n= 80 QDs, 8h n= 116 QDs, p= 0.36; **Passing**: t0 n= 78 QDs, 8h n= 90 QDs, p= 0.02. **(I)** Quantification of diffusion coefficients of α2 $GABA_AR$ after 48 h of 4-AP application. **Extra**: t0 n= 777 QDs, 48h n= 174 QDs, p= 0.69. **Syn**: t0 n= 126 QDs, 48h n= 213 QDs, p= $1.4\ 10^{-4}$. **(J)** Quantification of explored area EA of α2 $GABA_AR$ after 48 h of 4-AP application. **Extra**: t0 n= 2331 QDs, 48h n= 5508 QDs, p= 0.045. **Syn**: t0 n= 378 QDs, 48h n= 717 QDs, p= $2.2\ 10^{-20}$. (**K**) Quantification of α2 $GABA_AR$ dwell time after 48 h of 4-AP application. **Total**: t0 n= 201 QDs, 48h n= 254 QDs, p= 0.74. **Trapped**: t0 n= 91 QDs, 48h n= 110 QDs, p= 0.99. **Passing**: t0 n= 110 QDs, 48h n= 144 QDs, p= 0.81. In B-D, H, K, data are presented as mean ± SEM, *P≤0.05; ***P≤0.001 (Mann Whitney Rank sum test). In F-G, I-J, data are presented as median

values ± 25%-75% Interquartile Range IQR, *P≤0.05; ***P≤0.001 (Kolmogorov-Smirnov test). In B-G and I-J, values were normalized to the corresponding control values. In H, K, DT in s.

Figure 5: PKA and CaMKIIα signaling pathways regulate gephyrin clustering and α2 $GABA_AR$ membrane dynamics in conditions of chronic changes of activity. **(A)** Morphological analysis of neurons transfected with eGFP-S303A/S305A (eGFP-SSA) gephyrin double mutant insensitive to PKA and CaMKIIα signaling pathways. Double staining of VGAT (blue) and α2 $GABA_AR$ (red) at 21 DIV under control condition (t0) or in the presence of 4-AP for 48 h. Scale bar, 10 µm. **(B)** Quantifications of synaptic eGFP-SSA clusters and synaptic (α2 syn) and extrasynaptic (α2 extra) α2 $GABA_AR$ clusters in relation to eGFP-WT show minor impact of eGFP-SSA under control condition. eGFP-WT: n= 89 cells, eGFP-SSA n= 95 cells, 6 cultures. **eGFP-SSA**: Cluster Nb: p= 0.3; Area: p= 0.9; Intensity: p= 0.5. **α2 syn**: Cluster Nb: p= 0.4; Area: p= 0.5; Intensity: p= 0.8. **α2 extra**: Cluster Nb: p= 0.2; Area: p= 0.4; Intensity: p= 0.2. **(C)** Quantification of median diffusion coefficient D of α2 $GABA_AR$ in neurons expressing eGFP-WT or eGFP-SSA under control condition. **Extra**: WT n= 1166 QDs, SSA n= 989 QDs, p= $1.5\ 10^{-12}$; **Syn**: WT n= 312 QDs, SSA n= 245 QDs, p= 0.08; 4 cultures. **(D)** Quantification of median explored area EA of α2 $GABA_AR$ in neurons expressing eGFP-WT or eGFP-SSA under control condition. **Extra**: WT n= 3510 QDs, SSA n= 2778 QDs, p= $3.9\ 10^{-18}$; **Syn**: WT n= 932 QDs, SSA n= 735 QDs, p= $3.1\ 10^{-4}$. **(E)** Quantification of α2 $GABA_AR$ dwell time DT at synaptic sites in neurons expressing either eGFP-WT or eGFP-SSA. Calculations were done for all QDs (total), (trapped) or (passing) QDs at inhibitory synapses. No significant differences were found between eGFP-WT and eGFP-SSA. **Total**: WT n= 390 QDs, SSA n= 335 QDs,

p= 0.2; **Trapped**: WT n= 229 QDs, SSA n= 173 QDs, p= 0.4; **Passing**: WT n= 161 QDs, SSA n= 162 QDs, p= 0.9. **(F)** Quantification of eGFP-SSA clusters after 8 h and 48 h of 4-AP application. t0 n= 61 cells, 8h n= 52 cells, 48h n= 93 cells, 3-6 cultures. **Cluster Nb**: 0-8h: p= 0.2, 0-48h: p<0.001; **Area**: 0-8h: p= 0.8, 0-48h: p= 0.3; **intensity**: 0-8h: p= 0.8, 0-48h: p= 0.2. **(G)** Quantification of synaptic α2 $GABA_AR$ clusters after 8 h and 48 h of 4-AP compared with mock treated control. t0 n= 53 cells, 8h n= 50 cells, 48h n= 69 cells, 3-6 cultures. **Cluster Nb**: 0-8h: p<0.001, 0-48h: p<0.001; **Area**: 0-8h: p= 0.002, 0-48h: p= 0.09; **Intensity**: 0-8h: p= 0.5, 0-48h: p= 0.5. **(H)** Quantification of extrasynaptic α2 $GABA_AR$ clusters after 8 h and 48 h of 4-AP compared with mock treated control. **Cluster Nb**: 0-8h: p= 0.2, 0-48h: p= 0.1; **Area**: 0-8h: p=0.01, 0-48h: p= 0.9; **Intensity**: 0-8h: p= 0.002, 0-48h: p<0.001. (**I)** Quantification of α2 $GABA_AR$ diffusion coefficients in eGFP-SSA expressing cells after 8 h of 4-AP exposure. **Extra**: t0 n= 787 QDs, 4AP 8h n= 365 QDs, p= $3.6\ 10^{-4}$. **Syn**: t0 n= 212 QDs, 8h n= 187 QDs, p= 0.4; 5 cultures. (**J)** Quantification of explored area EA of α2 $GABA_AR$ after 8 h of 4-AP application. **Extra**: t0 n= 1869 QDs, 8h n= 1092 QDs, p= 0.002. **Syn**: t0 n= 753 QDs, 8h n= 558 QDs, p= 0.09. (**K)** Quantification of α2 $GABA_AR$ diffusion coefficients in eGFP-SSA expressing cells after 48 h of 4-AP exposure. **Extra:** t0 n= 1098 QDs, 4AP 48h n= 734 QDs, p= 0.002. **Syn:** t0 n= 287 QDs, 48h n= 198 QDs, p= 0.2; 5 cultures. (**L)** Quantification of explored area EA of α2 $GABA_AR$ after 48 h of 4-AP application. **Extra**: t0 n= 2169 QDs, 48h n= 1500 QDs, p= 0.04. **Syn**; t0 n= 633 QDs, 48h n= 510 QDs, p= 0.002. (**M)** Quantification of α2 $GABA_AR$ dwell time DT in neurons expressing eGFP-SSA after 8 h or 48 h of 4-AP application. Calculations were done for trapped or passing QDs at inhibitory synapses. T**rapped**: 8 h: n= 189 QDs, p= 0.3; 48 h: n= 166 QDs, p= 0.1; **Passing**: 8 h: n= 76 QDs, p= 0.3; 48 h: n= 132 QDs, p= 0.9. In B, E, F-H, M, data are presented as mean ±

SEM. **P<0.01; ***P≤0.001 (Mann Whitney Rank sum test). In C-D, I-L, data are presented as median values ± 25%-75% IQR; ***P≤0.001 (Kolmogorov-Smirnov test). In all graphs except E, values were normalized to the corresponding control values.

Figure 6: The ERK1/2 pathway does not influence structural synaptic adaptation. **(A)** Morphological analysis of eGFP-S268E in control (t0) or after 4-AP application for 8 h or 48 h. Scale bar, 10 µm. **(B)** Quantification of eGFP-S268E clusters after 8 h or 48 h of 4-AP application. t0 n= 50 cells, 8h n= 54 cells, 48h n= 55 cells, 3 cultures**.** **Cluster Nb**: 0-8h: p= 0.2, 0-48h: p= 0.004; **Area**: 0-8h: p= 0.02, 0-48h: p<0.001; **intensity**: 0-8h: p=0.003, 0-48h: p<0.001. 3 cultures. (**C**) Quantification of synaptic α2 $GABA_AR$ clusters after 8 h and 48 h of 4-AP compared with mock treated control. t0 n= 47 cells, 8h n= 50 cells, 48h n= 62 cells, 3-4 cultures. **Cluster Nb**: 0-8h: p= 0.08, 0-48h: p= 0.5; **Area**: 0-8h: p= 0.8, 0-48h: p= 0.03; **intensity**: 0-8h: p= 0.5, 0-48h: p<0.001. **(D)** Quantification of extrasynaptic α2 $GABA_AR$ clusters after 8 h and 48 h of 4-AP compared with mock treated control. **Cluster Nb**: 0-8h: p= 0.006, 0-48h: p= 0.007; **Area**: 0-8h: p= 0.02, 0-48h: p<0.001; **intensity**: 0-8h: p= 0.04, 0-48h: p<0.001. (**E**) Example traces of α2 $GABA_AR$ trajectories at extrasynaptic (extra) and synaptic (syn) sites under control condition (t0) or after 8 h or 48 h of 4-AP application. Scale bar, 0.25 µm. (**F)** Quantification of α2 $GABA_AR$ diffusion coefficients after 8 h of 4-AP exposure. **Extra**: t0 n= 1230 QDs, 4AP 8h n= 1855 QDs, p= $3.4\ 10^{-6}$. **Syn**: t0 n= 281 QDs, 8h n= 378 QDs, p= 0.2; 3 cultures. (**G)** Quantification of explored area EA of α2 $GABA_AR$ after 8 h of 4-AP application. **Extra**: t0 n= 3402 QDs, 8h n= 2454 QDs, p= $3.2\ 10^{-23}$. **Syn**: t0 n= 843 QDs, 8h n= 984 QDs, p= 0.02. (**H)** Quantification of α2 $GABA_AR$ diffusion coefficients after 48 h of 4-AP exposure. **Extra:** t0 n= 687 QDs, 4AP 48h n= 1611 QDs, p= 0.4. **Syn:** t0 n= 73 QDs, 48h n= 46 QDs, p= $1.6\ 10^{-4}$. (**I)**

Quantification of explored area EA of α2 $GABA_AR$ after 48 h of 4-AP application. **Extra**: t0 n= 2061 QDs, 48h n= 546 QDs, p= 2.9 10^{-6}. **Syn**; t0 n= 219 QDs, 48h n= 74 QDs, p= 6.6 10^{-7}. (**J)** Quantification of α2 $GABA_AR$ dwell time DT after 8 h or 48 h of 4-AP application. Calculations were done for trapped or passing QDs at inhibitory synapses. **Trapped**: t0: n= 130 QDs, 8 h: n= 194 QDs, p= 0.007; t0: n= 85 QDs, 48 h: n= 51 QDs, p= 0.02; **Passing**: t0: n= 91 QDs, 8 h: n= 161 QDs, p<0.001; t0: n= 91 QDs, 48 h: n= 31 QDs, p= 0.6. In B-D, J, data are presented as mean ± SEM. *P≤0.05; **P≤0.01; ***P≤0.001 (Mann Whitney Rank sum test). In F-I, data are presented as median values ± 25%-75% IQR. *P≤0.05; ***P≤0.001 (Kolmogorov-Smirnov test). In all graphs, values were normalized to the corresponding control values.

Figure 7: GSK3β pathway influences gephyrin scaffold and $GABA_ARs$ after changes in chronic activity. (**A**) Morphology of neuron transfected with eGFP-S270A under control condition (t0) or in the presence of 4-AP after 8 h or 48 h. Scale bar, 10 µm. **(B)** Quantification of eGFP-S270A clusters after 8 h or 48 h of 4-AP application. t0 n= 43 cells, 8h n= 50 cells; 48h n= 50 cells, 3 cultures**. Cluster Nb**: 0-8h: p= 0.8, 0-48h: p= 0.14; A**rea**: 0-8h: Mann Whitney test p= 0.7, 0-48h: p= 0.04; **Intensity**: 0-8h: p= 0.12, 0-48h: p<0.001. (**C**) Quantification of synaptic α2 $GABA_AR$ clusters after 8 h and 48 h of 4-AP compared with mock treated control. t0 n= 40 cells, 8h n= 47 cells; t0: n= 59 cells, 48h n= 52 cells, 3-5 cultures. **Cluster Nb**: 0-8h: p= 0.8, 0-48h: p= 0.7; A**rea**: 0-8h: p=0.14, 0-48h: p=0.6; **Intensity**: 0-8h: p=0.03, 0-48h: p=0.4. **(D)** Quantification of extrasynaptic α2 $GABA_AR$ clusters after 8 h and 48 h of 4-AP compared with mock treated control. **Cluster Nb**: 0-8h: p<0.001, 0-48h: p=0.7; **Area**: 0-8h: p<0.001, 0-48h: p=0.7; **Intensity**: 0-8h: p<0.001, 0-48h: p=0.3. (**E**) Example traces of α2 $GABA_AR$ trajectories at extrasynaptic (extra) and synaptic (syn) sites under

control conditions (t0) or after 8 h or 48 h of 4-AP application. Scale bar, 0.25 µm**.** (**F)** Quantification of α2 $GABA_AR$ diffusion coefficients after 8 h of 4-AP exposure. **Extra**: t0 n= 1580 QDs, 4AP 8h n= 1892 QDs, p= $1.4\ 10^{-13}$. **Syn**: t0 n= 229 QDs, 8h n= 307 QDs, p= $8.8\ 10^{-3}$; 3 cultures. (**G)** Quantification of explored area EA of α2 $GABA_AR$ after 8 h of 4-AP application. **Extra**: t0 n= 4575 QDs, 8h n= 4041 QDs, p= 0.02. **Syn**: t0 n= 687 QDs, 8h n= 663 QDs, p= 0.04. (**H)** Quantification of α2 $GABA_AR$ diffusion coefficients after 48 h of 4-AP exposure. **Extra:** t0 n= 314 QDs, 4AP 48h n= 338 QDs, p= 0.05. **Syn:** t0 n= 46 QDs, 48h n= 51 QDs, p= 0.04. 3 cultures. (**I)** Quantification of explored area EA of α2 $GABA_AR$ after 48 h of 4-AP application. **Extra**: t0 n= 939 QDs, 48h n= 771 QDs, p= 0.02. **Syn**; t0 n= 138 QDs, 48h n= 153 QDs, p= 0.04. (**J)** Quantification of α2 $GABA_AR$ dwell time DT after 8 h or 48 h of 4-AP application. Calculations were done for trapped or passing QDs at inhibitory synapses. **Trapped**: t0: n= 82 QDs, 8 h: n= 97 QDs, p= 0.04; t0: n= 191 QDs, 48 h: n= 45 QDs, p= 0.5; **Passing**: t0: n= 104 QDs, 8 h: n= 131 QDs, p= 0.5; t0: n= 211 QDs, 48 h: n= 23 QDs, p= 0.1. In B-D, J, data are presented as mean ± SEM. *P≤0.05; ***P≤0.001 (Mann Whitney Rank sum test). In F-I, data are presented as median values ± 25%-75% IQR. *P≤0.05; **P≤0.01; ***P≤0.001 (Kolmogorov-Smirnov test). In all graphs, values were normalized to the corresponding control values.

Figure 8: PKA, CAMKIIα and GSK3β pathways are required to tune the inhibitory synapse.

(**A**) Quantifications of synaptic eGFP-SSA/S270 clusters and synaptic (α2 syn) and extrasynaptic (α2 extra) α2 $GABA_AR$ clusters in relation to eGFP-WT show minor impact of the mutant under control condition. eGFP-WT n= 58 cells, eGFP-SSA/S270A n= 62 cells, 3 cultures. eGFP-SSA: **Cluster Nb**: p= 0.6; A**rea**: p= 0.1; **Intensity**: p=

0.7. α2 syn: **Cluster Nb**: p= 0.001; **Area**: p= 0.1; **Intensity**: p= 0.02. α2 extra: Cluster Nb: p= 0.03; **Area**: p= 0.5; **Intensity**: p= 0.2. **(B)** Quantification of median diffusion coefficient D of α2 $GABA_AR$ in neurons expressing eGFP-WT or eGFP-SSA/S270A under control condition. **Extra**: WT n= 823 QDs, SSA/S270A n= 786 QDs, p= 0.004; **Syn**: WT n= 261 QDs, SSA/S270A n= 211 QDs, p= 0.3, 2 cultures. **(C)** Quantification of α2 $GABA_AR$ dwell time DT at synaptic sites in neurons expressing either eGFP-WT or eGFP-SSA/S270A. Calculations were done for all QDs (total), (trapped) or (passing) QDs at inhibitory synapses. No significant differences were found between eGFP-WT and eGFP-SSA/S270A. **Total**: WT n= 165 QDs, SSA/S270A n= 183 QDs, p= 0.1; **Trapped**: WT n= 95 QDs, SSA/S270A n= 116 QDs, p= 0.5; **Passing**: WT n= 70 QDs, SSA/S270A n= 67 QDs, p= 0.2. **(D)** Quantification of eGFP-SSA/S270A clusters after 8 h or 48 h of 4-AP application. t0 n= 53 cells, 8h n= 45 cells, 48h n= 51 cells, 3 cultures**. Cluster Nb**: 0-8h: p= 0.3, 0-48h: p<0.001; **Area**: 0-8h: p= 0.03, 0-48h: p= 0.2; **Intensity**: 0-8h: p= 0.3, 0-48h: p= 0.9. (**E**) Quantification of synaptic α2 $GABA_AR$ clusters after 8 h and 48 h of 4-AP compared with mock treated control. t0 n= 49 cells, 8h n= 49 cells, 48h n= 39 cells, 3 cultures. **Cluster Nb**: 0-8h: p= 0.2, 0-48h: p<0.001; **Area**: 0-8h: p= 0.8, 0-48h: p= 0.6; **Intensity**: 0-8h: p= 0.2, 0-48h: p= 0.9. **(F)** Quantification of extrasynaptic α2 $GABA_AR$ clusters after 8 h and 48 h of 4-AP compared with mock treated control. **Cluster Nb**: 0-8h: p= 0.8, 0-48h: p= 0.001; **Area**: 0-8h: p<0.001, 0-48h: p= 0.7; **Intensity**: 0-8h: p= 0.8, 0-48h: p= 0.8. (**G)** Quantification of α2 $GABA_AR$ diffusion coefficients after 8 h of 4-AP exposure. **Extra**: t0 n= 624 QDs, 4AP 8h n= 421 QDs, p= 5.4 10^{-7}. **Syn**: t0 n= 252 QDs, 8h n= 173 QDs, p= 0.2, 2 cultures. (**H)** Quantification of explored area EA of α2 $GABA_AR$ after 8 h of 4-AP application. **Extra**: t0 n= 1869 QDs, 8h n= 1092 QDs, p= 7.8 10^{-14}. **Syn**: t0 n= 753 QDs, 8h n= 516 QDs, p= 0.07. (**I)** Quantification of α2 $GABA_AR$ diffusion

coefficients after 48 h of 4-AP exposure. **Extra:** t0 n= 624 QDs, 4AP 48h n= 631 QDs, p= 0.04. **Syn:** t0 n= 252 QDs, 48h n= 251 QDs, p= 0.8. 2 cultures. (**J)** Quantification of explored area EA of α2 $GABA_AR$ after 48 h of 4-AP application. **Extra**: t0 n= 1092 QDs, 48h n= 1890 QDs, p= $1.5\ 10^{-6}$. **Syn**; t0 n= 558 QDs, 48h n= 750 QDs, p= 0.3. (**K)** Quantification of α2 $GABA_AR$ dwell time DT after 8 h or 48 h of 4-AP application. Calculations were done for trapped or passing QDs at inhibitory synapses. **Trapped**: t0: n= 116 QDs, 8 h: n= 84 QDs, 48 h: n= 43 QDs, 0-8h: p= 0.2; 0-48h: p= 0.02; **Passing**: t0: n= 67 QDs, 8 h: n= 46 QDs, 48 h: n= 43 QDs, 0-8h: p= 0.2; 0-48h: p= 0.1. In A, C-F, K, data are presented as mean ± SEM. *P≤0.05; ***P≤0.001 (Mann Whitney Rank sum test). In G-J, data are presented as median values ± 25%-75% IQR. *P≤0.05; ***P≤0.001 (Kolmogorov-Smirnov test). In all graphs except in C, values were normalized to the corresponding control values.

Figure 1

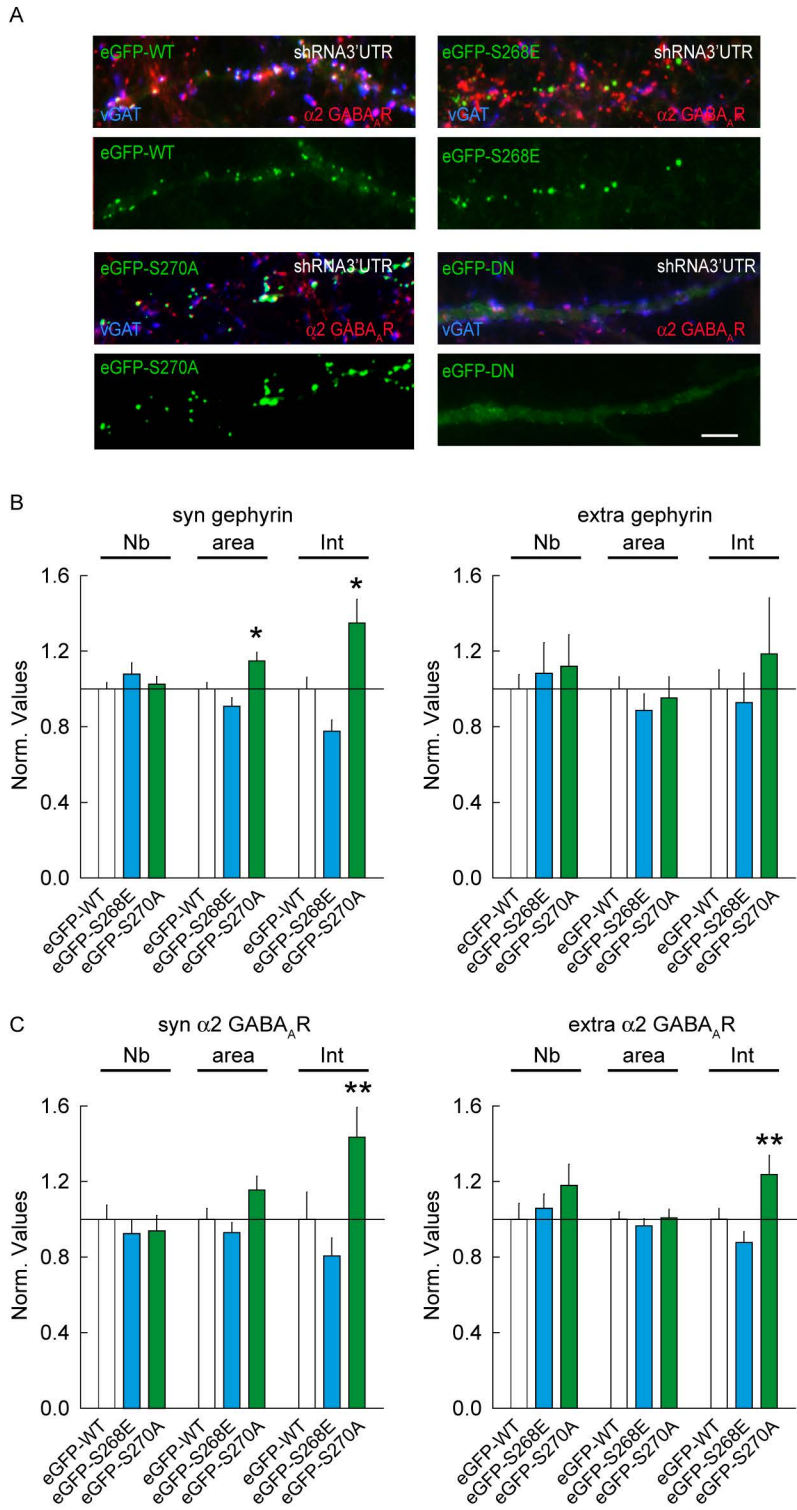
A
eGFP-WT
shRNA3'UTR
vGAT
α2 GABA$_A$R
eGFP-S268E
eGFP-S270A
eGFP-DN
B
syn gephyrin
extra gephyrin
Nb
area
Int
Norm. Values
1.6
1.2
0.8
0.4
0.0
*
eGFP-WT
eGFP-S268E
eGFP-S270A
C
syn α2 GABA$_A$R
extra α2 GABA$_A$R
**

Figure 2

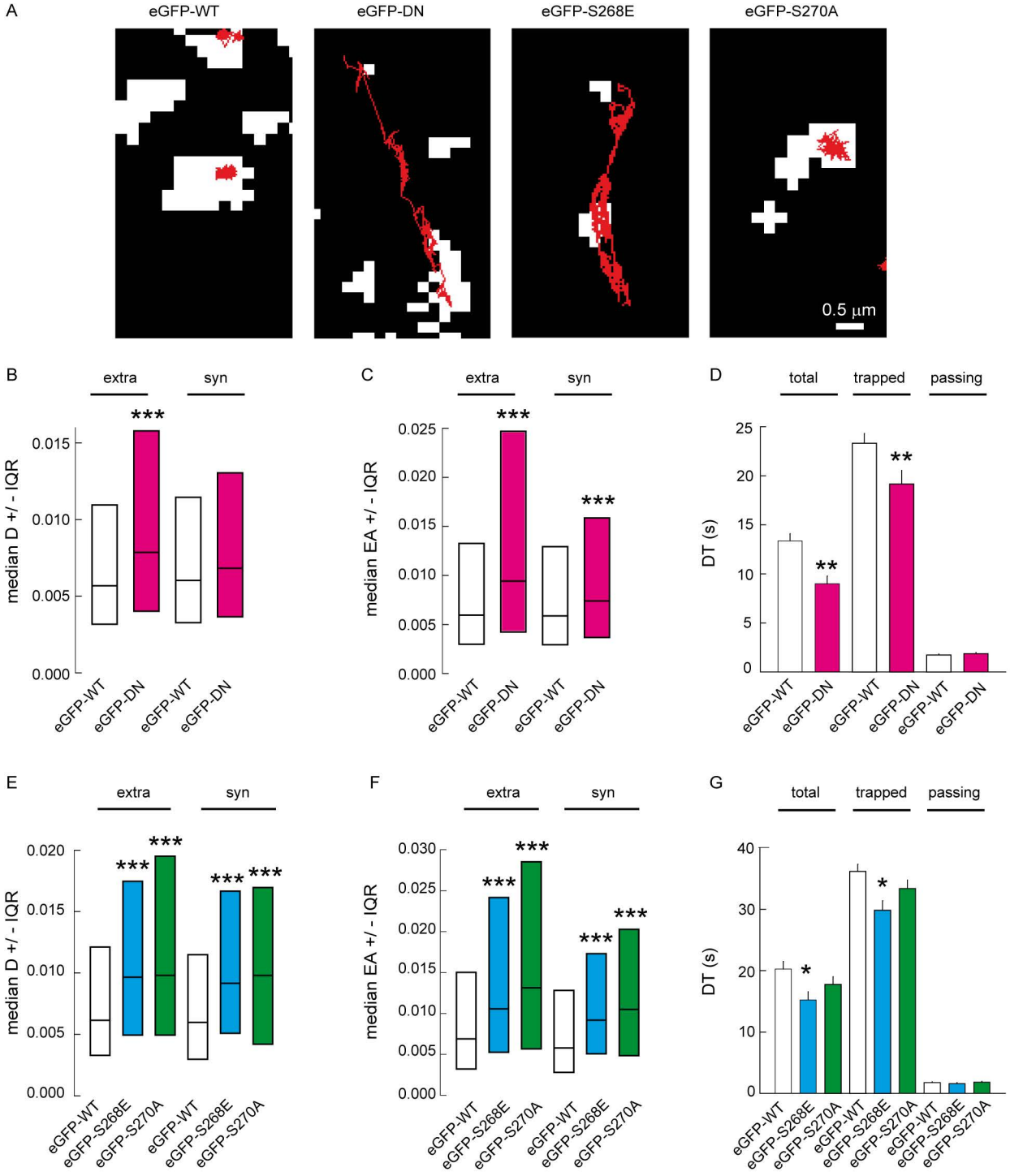
A
eGFP-WT
eGFP-DN
eGFP-S268E
eGFP-S270A
0.5 µm
B
extra
syn
median D +/- IQR
0.000
0.005
0.010
0.015
***
eGFP-WT
eGFP-DN
eGFP-WT
eGFP-DN
C
extra
syn
median EA +/- IQR
0.000
0.005
0.010
0.015
0.020
0.025
***
***
eGFP-WT
eGFP-DN
eGFP-WT
eGFP-DN
D
total
trapped
passing
DT (s)
0
5
10
15
20
25
**
**
eGFP-WT
eGFP-DN
eGFP-WT
eGFP-DN
eGFP-WT
eGFP-DN
E
extra
syn
median D +/- IQR
0.000
0.005
0.010
0.015
0.020
***
***
***
***
eGFP-WT
eGFP-S268E
eGFP-S270A
eGFP-WT
eGFP-S268E
eGFP-S270A
F
extra
syn
median EA +/- IQR
0.000
0.005
0.010
0.015
0.020
0.025
0.030
***
***
***
***
eGFP-WT
eGFP-S268E
eGFP-S270A
eGFP-WT
eGFP-S268E
eGFP-S270A
G
total
trapped
passing
DT (s)
0
10
20
30
40
*
*
eGFP-WT
eGFP-S268E
eGFP-S270A
eGFP-WT
eGFP-S268E
eGFP-S270A
eGFP-WT
eGFP-S268E
eGFP-S270A

Figure 4

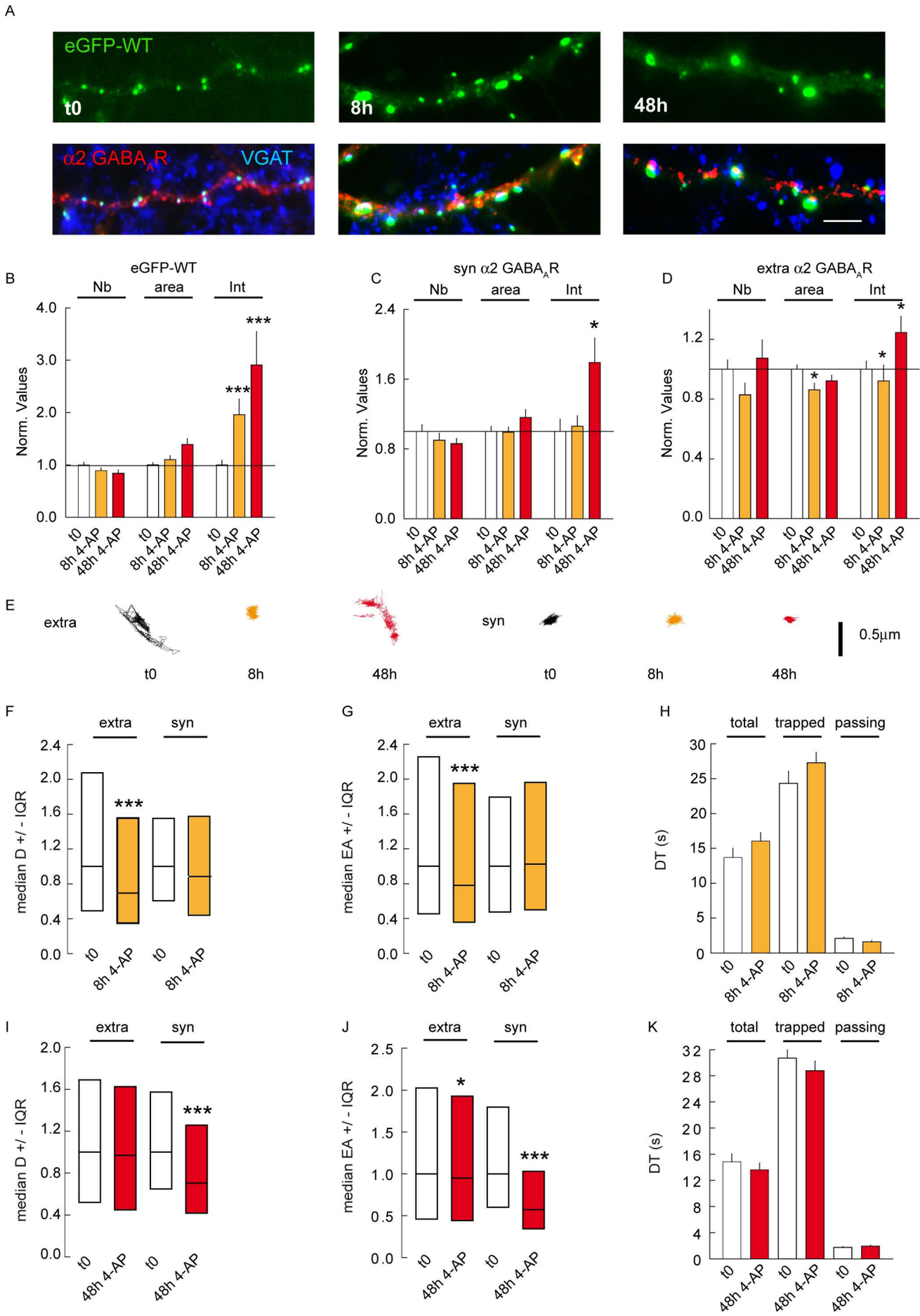
A
eGFP-WT
t0
8h
48h
α2 GABA$_A$R
VGAT
B
eGFP-WT
Nb
area
Int
Norm. Values
4.0
3.0
2.0
1.0
0.0
***
***
t0
8h 4-AP
48h 4-AP
C
syn α2 GABA$_A$R
Nb
area
Int
Norm. Values
2.4
1.6
0.8
0.0
*
D
extra α2 GABA$_A$R
Nb
area
Int
Norm. Values
1.2
0.8
0.4
0.0
*
*
*
E
extra
syn
0.5µm
t0
8h
48h
t0
8h
48h
F
extra
syn
median D +/- IQR
2.4
2.0
1.6
1.2
0.8
0.4
0.0
***
t0
8h 4-AP
G
extra
syn
median EA +/- IQR
2.4
2.0
1.6
1.2
0.8
0.4
0.0
***
H
total
trapped
passing
DT (s)
30
25
20
15
10
5
0
I
extra
syn
median D +/- IQR
2.0
1.6
1.2
0.8
0.4
0.0
***
48h 4-AP
J
extra
syn
median EA +/- IQR
2.5
2.0
1.5
1.0
0.5
0.0
*
***
K
total
trapped
passing
DT (s)
32
28
24
20
16
12
8
4
0

Figure 3

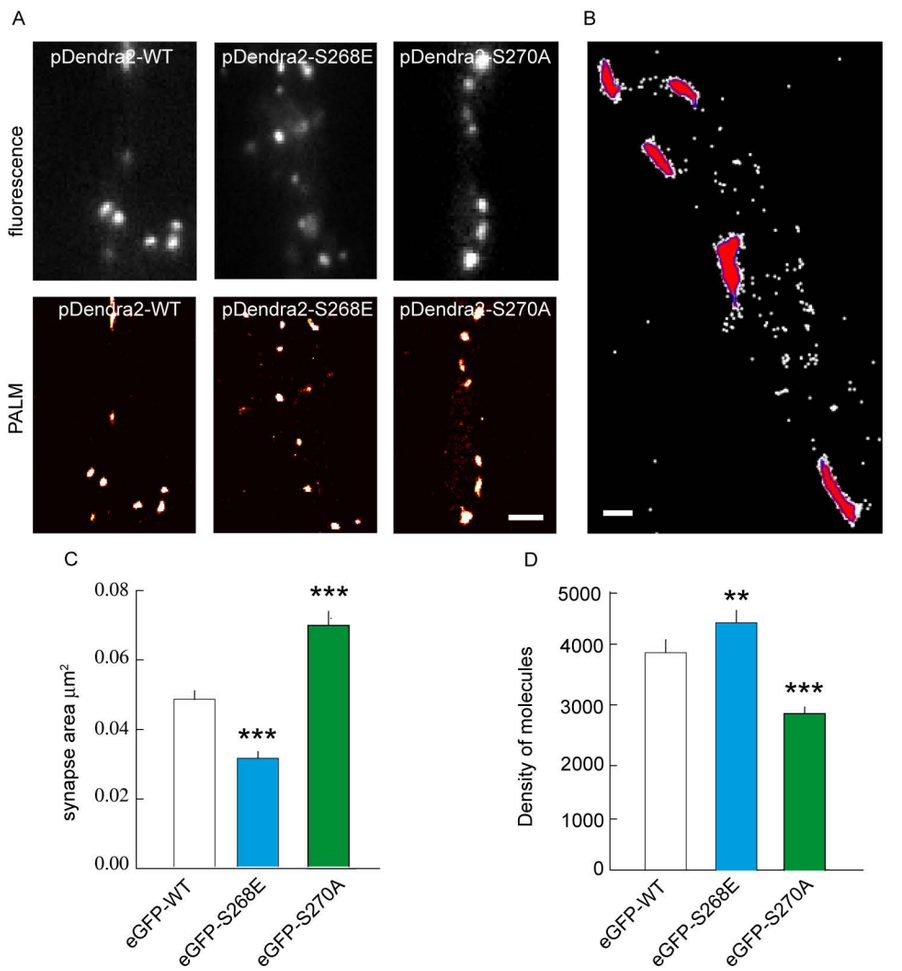
A
B
fluorescence
PALM
pDendra2-WT
pDendra2-S268E
pDendra2-S270A
pDendra2-WT
pDendra2-S268E
pDendra2-S270A
C
synapse area µm²
0.08
0.06
0.04
0.02
0.00
***
***
eGFP-WT
eGFP-S268E
eGFP-S270A
D
Density of molecules
5000
4000
3000
2000
1000
0
**
***
eGFP-WT
eGFP-S268E
eGFP-S270A

Figure 5

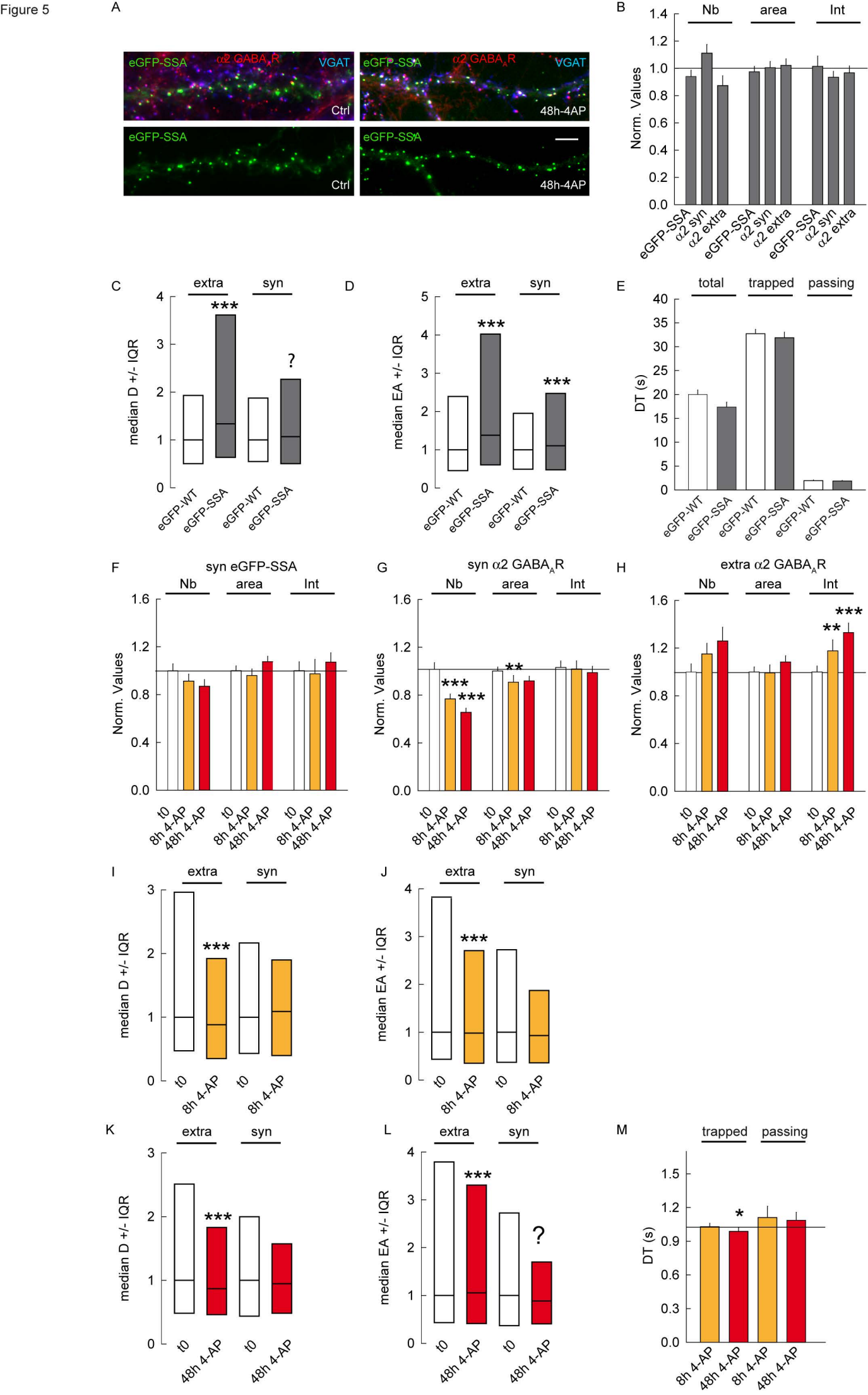
A
eGFP-SSA
α2 GABA$_A$R
VGAT
Ctrl
48h-4AP
B
Nb
area
Int
Norm. Values
eGFP-SSA
α2 syn
α2 extra
C
extra
syn
median D +/- IQR
eGFP-WT
eGFP-SSA
D
median EA +/- IQR
E
total
trapped
passing
DT (s)
F
syn eGFP-SSA
t0
8h 4-AP
48h 4-AP
G
syn α2 GABA$_A$R
H
extra α2 GABA$_A$R
I
J
K
48h 4-AP
L
M

Figure 6

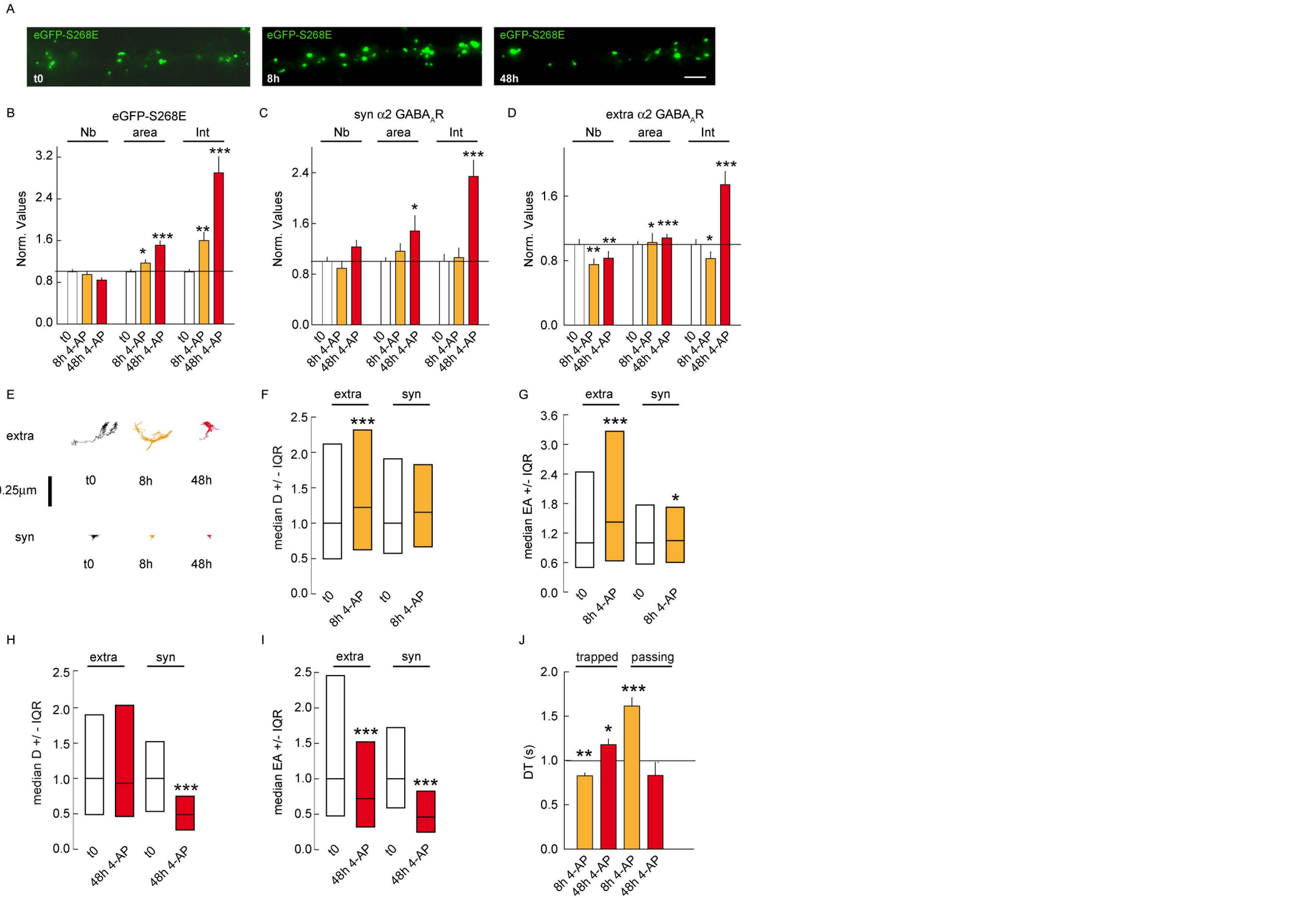
A
eGFP-S268E
t0
eGFP-S268E
8h
eGFP-S268E
48h
B
eGFP-S268E
Nb
area
Int
Norm. Values
t0
8h 4-AP
48h 4-AP
C
syn α2 GABA$_A$R
D
extra α2 GABA$_A$R
E
extra
0.25µm
syn
t0
8h
48h
F
extra
syn
median D +/- IQR
G
median EA +/- IQR
H
48h 4-AP
I
J
trapped
passing
DT (s)

Figure 7

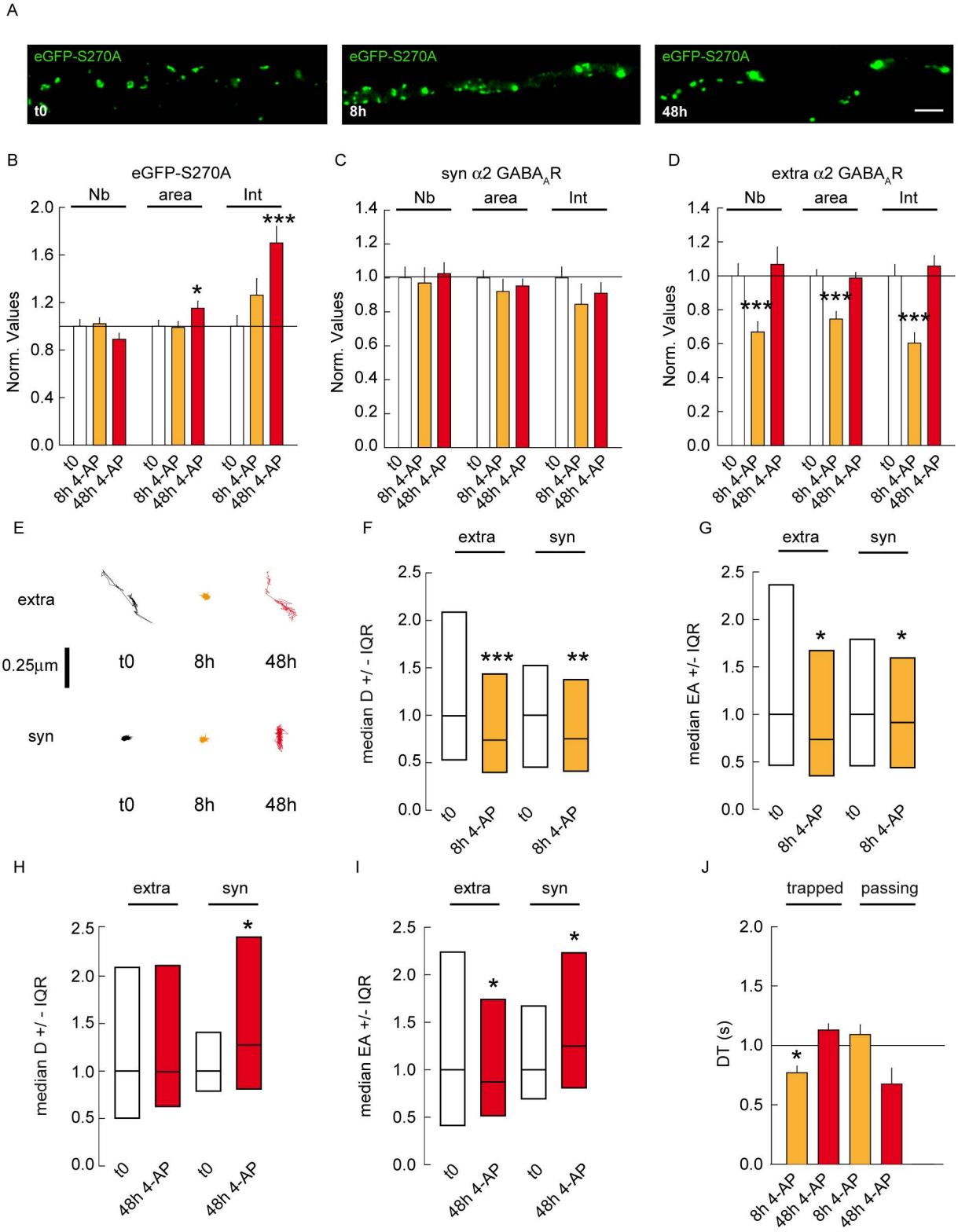
A
eGFP-S270A
t0
eGFP-S270A
8h
eGFP-S270A
48h
B
eGFP-S270A
Nb
area
Int
Norm. Values
t0
8h 4-AP
48h 4-AP
C
syn α2 GABA$_A$R
D
extra α2 GABA$_A$R
E
extra
0.25µm
t0
8h
48h
syn
F
extra
syn
median D +/- IQR
G
median EA +/- IQR
H
48h 4-AP
I
J
trapped
passing
DT (s)

Figure 8

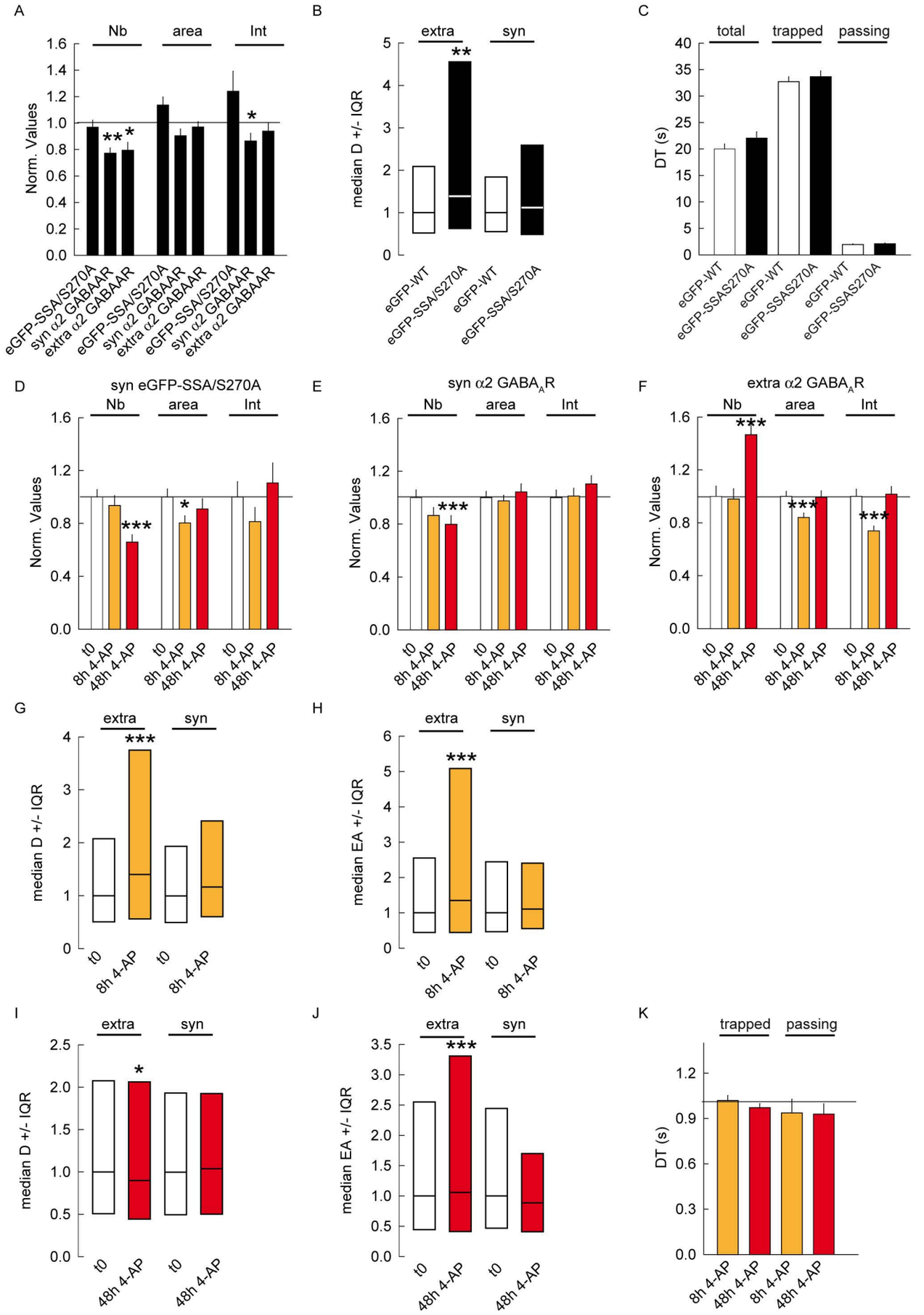
A
Nb
area
Int
Norm. Values
eGFP-SSA/S270A
syn α2 GABAAR
extra α2 GABAAR
B
extra
syn
median D +/- IQR
eGFP-WT
eGFP-SSA/S270A
C
total
trapped
passing
DT (s)
eGFP-SSAS270A
D
syn eGFP-SSA/S270A
t0
8h 4-AP
48h 4-AP
E
syn α2 GABA$_A$R
F
extra α2 GABA$_A$R
G
H
median EA +/- IQR
I
J
K